American Mineralogist, Volume 59, pages 729–762, 1974

Review of Metamorphic Mixed-Volatile (H_2O-CO_2) Equilibria

DERRILL M. KERRICK

Department of Geosciences, The Pennsylvania State University, University Park, Pennsylvania 16802

Abstract

The slopes and curvatures of various types of mixed-volatile (H_2O-CO_2) equilibria on T-X diagrams can be readily interpreted by considering the change in chemical potentials of volatile components as a function of activity. T-X equilibria can be extrapolated with sufficient accuracy from a narrow experimental bracket, using an equation assuming constant ΔH_r and accounting for non-ideal mixing in the fluid phase. Positive deviations from ideal mixing in the fluid, as measured experimentally, will flatten the extrapolated T-X curves of various types of mixed-volatile equilibria in comparison to the curves for ideal mixing. Addition of CH_4 to the fluid, as with graphite-bearing systems, would alter the T-X projections of most types of mixed-volatile reactions.

Mixed-volatile equilibria can also be analyzed with isobaric, isothermal $\mu_{H_2O} - \mu_{CO_2}$ (or log f_{H_2O} — log f_{CO_2}) diagrams. The main advantage of such diagrams over T-X plots is that vapor-deficient systems can be investigated.

Critical evaluation of experimental data on mixed-volatile equilibria must include an estimate of the sensitivity of the experimental technique, the amount of reaction which occurred, possible nucleation of unwanted phases, and total errors in measurement of P, T, and X_{CO_2}. Considering potential problems with any single experimental method, a particular mixed-volatile reaction should be investigated by several independent techniques.

T-X topologies for various chemical systems show numerous minerals or mineral assemblages which are excellent indicators of fluid composition during metamorphism. For example, grossularite, zoisite, margarite, prehnite, lawsonite, brucite, and serpentine indicate extremely H_2O-rich fluids, whereas dolomite + diopside, anthophyllite + magnesite, and, at moderate temperatures, dolomite + quartz, indicate CO_2-rich fluids. Pressure variation may profoundly affect T-X topologies, as in the system MgO-SiO_2-CO_2-H_2O.

Complications in applying experimentally-derived mixed-volatile equilibria to natural systems may occur if the fluid pressure (P_f) is less than the solid (lithostatic) pressure (P_s), and the fluid departs from a binary H_2O-CO_2 composition. It is reasonable to assume that rapid recrystallization, coupled with devolatilization reactions, would maintain $P_f \simeq P_s$ in many metamorphic systems. The presence of a vapor phase is suggested by fluid inclusions, veins filled with metamorphic minerals, and abundance of fluids permeating rocks undergoing contemporary metamorphism. The role of solid solution must be considered in any field investigation of mixed-volatile equilibria. The effect of solid solution on T-X equilibria can be calculated by ideal solid solution models, or, better, calculations involving activities of solid phases. Non-binary fluids will be most important in graphite-bearing systems—increasing departure from a binary H_2O-CO_2 fluid will occur in graphitic systems with decrease in f_{O_2}. Non-ideal mixing becomes most important in low-grade metamorphic regimes; unmixing of H_2O and CO_2 at low temperatures further complicates mixed-volatile equilibria in low-grade metamorphism.

Both "open" and "closed" behavior of metamorphic systems with regard to H_2O and CO_2 have been described; in addition, some field studies have shown a change from closed to open behavior with time. No generalizations can be made as to favoring open *vs* closed behavior, such that each geologic system must be independently evaluated.

Silicate mineralogy in calcareous metasomatic rocks, such as skarns and rodingites, suggest the presence of H_2O-rich fluids during formation. The lack of buffer assemblages in skarns is compatible with open behavior with regard to volatiles, a consequence of the large influx of H_2O from the adjacent intrusive.

Symbols

a_i = activity of species (i)
Cp = heat capacity at constant pressure
f_i^* = fugacity of species (i) in mixture
f_i^0 = fugacity of pure species (i)
γ_i = fugacity coefficient of species (i)
$\bar{G}_i$ = partial molal free energy of species (i)
ΔG_r = free energy change of a reaction
ΔH_r = enthalpy change of a reaction
i = chemical species (*e.g.*, H_2O, CO_2)
K = equilibrium constant
n_i = stoichiometric coefficient of species (i) in a balanced reaction
N_i = number of moles of species (i)
^{0} = *superscript* referring to standard state (taken as the pure substance at P and T)
P_f = fluid pressure
P_s = solid (lithostatic) pressure
$\bar{S}_i$ = partial molal entropy of component i
ΔS_r = entropy change of reaction
T = temperature
ΔV_r = volume change of reaction
X_i = mole fraction of species (i)
$_{1,2}$ = *subscripts* referring to limits of integration
μ_i = chemical potential of species (i)

Introduction

In 1962, H. J. Greenwood and P. J. Wyllie independently published short notes which spurred numerous field and experimental investigations on the role of H_2O-CO_2 mixtures in metamorphic equilibria. To many petrologists this approach was a welcome addition since it provided an improved model for the interpretation of natural systems. The present paper reviews investigations on mixed-volatile equilibria and emphasizes the strengths and weaknesses of applying experimentally-derived results to natural systems. This review is primarily intended for those who are relatively unfamiliar with mixed-volatile equilibria, although the reference list and diagrams will hopefully be useful to those now engaged in research on this subject.

Theory

Thermodynamics of Mixed-Volatile Equilibria

In discussing mixed-volatile equilibria it is useful to classify five types of reactions: ⟨1⟩ $A = B$; ⟨2⟩ $A = B + CO_2$; ⟨3⟩ $A = B + H_2O$; ⟨4⟩ $A = B + CO_2 + H_2O$; ⟨5⟩ $A + CO_2 = B + H_2O$. Here, A and B refer to either a solid phase or an assemblage of solid phases. For all reactions a general expression can be written as:

$$A = B + n_{H_2O}H_2O + n_{CO_2}CO_2,$$

where $n_{H_2O} = n_{CO_2} = 0$ in reaction ⟨1⟩, $n_{H_2O} = 0$ in reaction ⟨2⟩, and $n_{CO_2} = 0$ in reaction ⟨3⟩; for reaction ⟨5⟩ the last term in the above expression would be negative because of transposition of CO_2 to the right side of the equation[1]. A useful thermodynamic expression relating the equilibrium free energy change of this general reaction as a function of intensive variables was derived by Greenwood (1967a, p. 545):

$$d\Delta G_r = \Delta V_r^0\, dP - \Delta S_r^0\, dT + d(RT \ln a_{H_2O}^{n_{H_2O}} \cdot a_{CO_2}^{n_{CO_2}}) = 0 \quad \text{Eq. (a)}$$

For the moment we will assume ideal *mixing* in the fluid phase[2],

$$\left(\frac{f_i^*}{f_i^0}\right)_{P,T} = a_i = X_i,$$

which yields,

$$\Delta V_r^0\, dP - \Delta S_r^0\, dT + n_{H_2O}\, d(RT \ln X_{H_2O}) + n_{CO_2}\, d(RT \ln X_{CO_2}) = 0 \quad \text{Eq. (b)}$$

An integrated form of this expression would generate the equilibrium surface of a reaction in P-T-X_{CO_2} space (Fig. 1a). Although a three-dimensional P-T-X_{CO_2} diagram is instructive, graphical portrayal is easier by considering sections through this diagram at constant X_{CO_2}, T or P. (Figs. 1b, 1c, 1d). The variation in equilibrium temperature with X_{CO_2} is shown in the T-X_{CO_2} diagram (Fig. 1d) as traces of the equilibrium curves at pressures P_1, P_2, and P_3. The equation for the slope of such equilibrium curves for an isobaric section can be derived from equation (b) with $dP = 0$, which yields:

$$-\Delta S_r^0\, dT + \frac{n_{H_2O}RT\, dX_{H_2O}}{X_{H_2O}} + n_{H_2O}R \ln X_{H_2O} dT + \frac{n_{CO_2}RT\, dX_{CO_2}}{X_{CO_2}} + n_{CO_2}R \ln X_{CO_2}\, dT = 0$$

[1] By the same argument, the term: n_{H_2O} H_2O, would be negative if the reaction were written with H_2O on the left side.

[2] Ideal *mixing* [where $(d\gamma_i/dX_i)_{P,T} = 0$] is clearly independent of ideality of the pure gas species at P and T.

Since: $dX_{H_2O} = -dX_{CO_2}$, and writing:

$$\Delta S_r = \Delta S_r^0 - n_{H_2O}R \ln X_{H_2O} - n_{CO_2}R \ln X_{CO_2} \qquad \text{Eq. (c)}$$

we obtain:

$$-\Delta S_r\, dT - \frac{n_{H_2O}RT\, dX_{CO_2}}{X_{H_2O}} + \frac{n_{CO_2}RT\, dX_{CO_2}}{X_{CO_2}} = 0,$$

which yields the slope equation:

$$\frac{dT}{dX_{CO_2}} = \frac{RT}{\Delta S_r}\left[\frac{n_{CO_2}}{X_{CO_2}} - \frac{n_{H_2O}}{X_{H_2O}}\right]$$

$$= \frac{RT^2}{\Delta H_r}\left[\frac{n_{CO_2}}{X_{CO_2}} - \frac{n_{H_2O}}{X_{H_2O}}\right] \qquad \text{Eq. (d)}$$

The equivalent expressions involving entropy and enthalpy in this equation are linked by:

$$\Delta G_r = 0 = \Delta H_r - T\Delta S_r,$$

or:

$$\Delta H_r = T\Delta S_r$$

Equation (d) is identical to that derived by Greenwood (1967a). From this expression the relative magnitudes of the slopes of various equilibria on a T-X_{CO_2} diagram can be deduced by comparison of ΔS_r, such that large values of ΔS_r yield flat slopes, and small values of ΔS_r produce steep slopes.

Figure 2 illustrates the relative slopes and curvatures of equilibria ⟨1⟩–⟨5⟩. Solid-solid equilibria (type ⟨1⟩) will plot as a horizontal line on this diagram;

Abbreviations for Minerals in Figures

A = anthophyllite	Di = diopside	K-fs = K-feldspar	Qz, Q = quartz
An = anorthite	Dol, Do = dolomite	M = magnesite	S = serpentine
And = andalusite	E = enstatite	Ma = margarite	T, Tc = talc
B = brucite	F, Fo = forsterite	P = periclase	Tr = tremolite
Cal, Cc = calcite	Ge = gehlenite	Ph = phlogopite	Wo = wollastonite
Co = corundum	Gr = grossularite	Pr = prehnite	Zo = zoisite

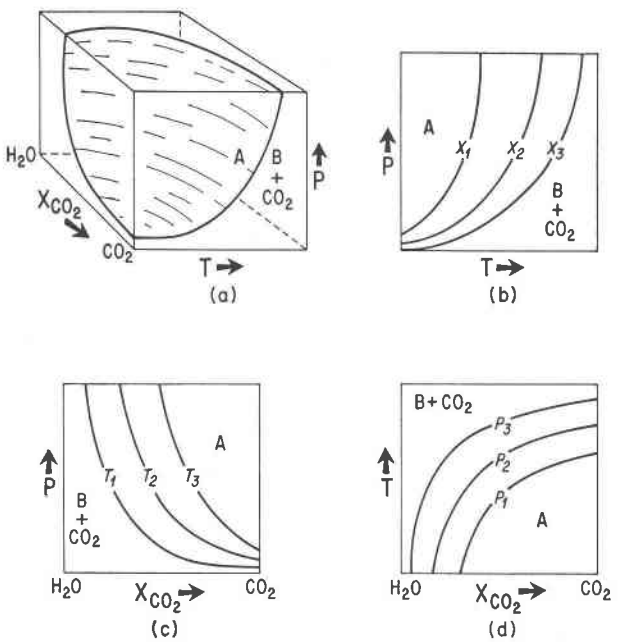

FIG. 1. (a) Schematic P-T-X_{CO_2} volume showing the equilibrium surface for a decarbonation reaction. (b) P-T projection of reaction showing lines for three fixed values of X_{CO_2} ($X_1 < X_2 < X_3$). (c) P-X_{CO_2} projection of reaction showing lines for three fixed temperatures ($T_1 < T_2 < T_3$). (d) T-X_{CO_2} projection of reaction showing lines for three fixed pressures ($P_1 < P_2 < P_3$).

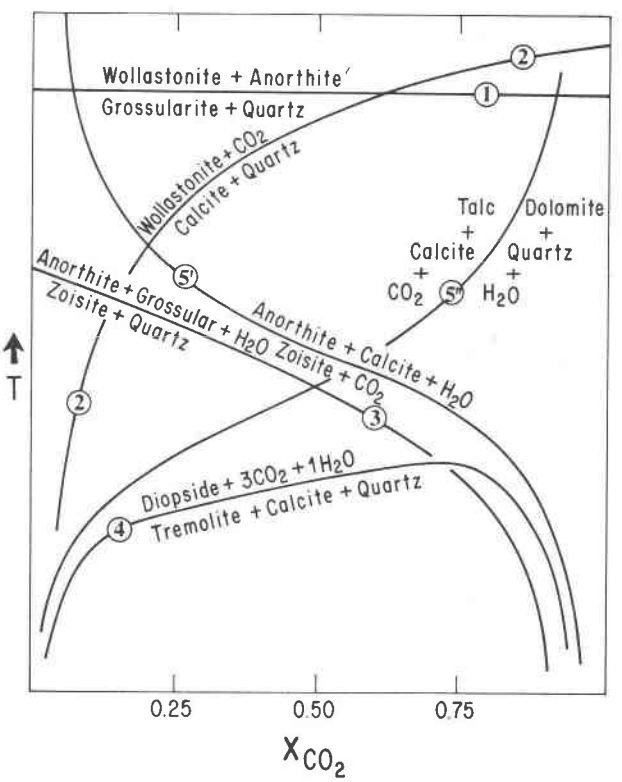

FIG. 2. Schematic illustrations of various types of mixed-volatile equilibria on a T-X_{CO_2} diagram.

obviously, because no volatiles are involved in the reaction, the equilibrium temperature will be unaffected by changes in the fluid composition. Although the slopes and curvatures of all mixed-volatile equilibria can be rationalized with equation (d), as was done by Greenwood (1962, 1967a), an alternative approach is to examine these reactions in terms of the chemical potentials of the fluid components. Rearranging Eq. (a) at constant pressure,

$$\Delta S_r^0\, dT = n_{H_2O}\, d(RT \ln a_{H_2O}) + n_{CO_2}\, d(RT \ln a_{CO_2})$$

With the entropy term as in Eq. (c),

$$dT = \frac{n_{H_2O} RT\, d \ln a_{H_2O}}{\Delta S_r} + \frac{n_{H_2O} RT\, d \ln a_{CO_2}}{\Delta S_r}$$

Since $d\bar{G}_i = d\mu_i = RT\, d \ln a_i$,

$$dT = \frac{n_{H_2O}\, d\mu_{H_2O}}{\Delta S_r} + \frac{n_{CO_2}\, d\mu_{CO_2}}{\Delta S_r} \qquad \text{Eq. (e)}$$

Upon integration:

$$\Delta T = \frac{n_{H_2O}\, \Delta\mu_{H_2O}}{\Delta S_r} + \frac{n_{CO_2}\, \Delta\mu_{CO_2}}{\Delta S_r}$$

For reaction ⟨2⟩ the term involving $\Delta\mu_{H_2O}$ becomes zero, whereas the term with $\Delta\mu_{CO_2}$ is zero in reaction ⟨3⟩. Thus, the temperature lowering of reaction ⟨2⟩ with decreasing X_{CO_2} reflects the increasingly negative $\Delta\mu_{CO_2}$ with lowering X_{CO_2}. Because ΔT is a logarithmic function of X_{CO_2}, the equilibrium curve will be concave downward. Furthermore, this equilibrium will be asymptotic to the left margin of the diagram ($X_{CO_2} = 0$) since $\lim_{x \to 0} (\ln X) = -\infty$. This asymptotic relation is further evident because a carbonate (and, thus, the assemblage calcite + quartz in Figure 2) would not be stable in a vapor phase with $X_{CO_2} = 0$ (*i.e.*, $P_{CO_2} = 0$). Since type ⟨3⟩ equilibria evolve only H_2O, similar reasoning suggests a concave-downward curve of negative slope which is asymptotic to the right margin ($X_{CO_2} = 1$). This is compatible with the fact that a hydrous phase (in this case zoisite) would be unstable in the presence of pure CO_2. Reaction ⟨4⟩ is concave downward with a maximum temperature at:

$$X_{CO_2} = \frac{n_{CO_2}}{n_{H_2O} + n_{CO_2}}$$

This maximum results from solution of equation (d) with:

$$\left(\frac{dT}{dX_{CO_2}}\right) = 0$$ (*i.e.*, a horizontal tangent to the curve).

The strong curvature in the extremes of X_{CO_2} reflects the large negative $\Delta\mu_{CO_2}$ at low X_{CO_2}, and a large negative $\Delta\mu_{H_2O}$ in the high X_{CO_2} range. The asymptotic approach of this reaction to the left *and* right sides of the diagram is compatible with the presence of *both* a hydrous phase and a carbonate in the low temperature assemblage. Equilibria of type ⟨5⟩ have an "S" shape on a T-X_{CO_2} plot, and toward higher temperature are either asymptotic to the left margin of the diagram (reaction ⟨5′⟩ in Figure 2) or to the right (reaction ⟨5″⟩ in Figure 2). In both cases H_2O appears on the right side of the curve whereas CO_2 is on the left, in conformance with the fact that a particular gas component (H_2O or CO_2) will be liberated into the vapor phase under reduced activity of this component. Furthermore the asymptotic approach to the left and right margins of type ⟨5⟩ reactions reflects $\Delta\mu$ of the volatile species in the extremes of X_{CO_2}; for example, with reaction ⟨5′⟩ at low X_{CO_2}, the large negative $\Delta\mu_{CO_2}$ expands the temperature of the left side of the reaction, which contains CO_2, whereas at high X_{CO_2} the large negative $\Delta\mu_{H_2O}$ expands the stability of anorthite + calcite + H_2O. The same reasoning is applicable to the asymptotic nature of equilibria ⟨5″⟩ at extremes of X_{CO_2}. Type ⟨5⟩ equilibria with equal absolute values of n_{H_2O} and n_{CO_2} are steeper on T-X diagrams than other mixed-volatile reactions because volatiles appear on opposite sides of the reaction, so that ΔS_r is relatively small. Where $|n_{H_2O}|$ and $|n_{CO_2}|$ differ, the direction of curvature of equilibrium ⟨5⟩ can usually be determined by inspection since, in comparing $|n_{H_2O}|$ and $|n_{CO_2}|$, the high temperature (= high entropy) assemblage contains the larger number of moles of gas species. Thus, where $|n_{H_2O}| > |n_{CO_2}|$ the curvature will be of type ⟨5′⟩, whereas with $|n_{H_2O}| < |n_{CO_2}|$ the curvature will be as ⟨5″⟩. However, where $|n_{H_2O}| = |n_{CO_2}|$ [such as the specific reaction ⟨5′⟩ shown in Figure 2] the high entropy assemblage cannot be determined by inspection of the stoichiometry; thus, it is necessary to calculate ΔS_r at a fixed T-X_{CO_2} point to determine which assemblage is the high entropy (*i.e.*, high temperature) side. In such a case, if H_2O is on the high entropy side, the curve has a negative slope, whereas the curve has a positive slope if H_2O occurs in the low entropy assemblage. The inflection point for type ⟨5⟩ equilibria can be determined by taking the second derivative of equation (d) (Greenwood, 1967a):

$$\left(\frac{d^2T}{dX_{CO_2}^2}\right) = 0 = -\left[\frac{n_{CO_2}}{X_{CO_2}^2} + \frac{n_{H_2O}}{X_{H_2O}^2}\right] + \frac{2RT}{\Delta H_r}\left[\frac{n_{CO_2}}{X_{CO_2}} - \frac{n_{H_2O}}{X_{H_2O}}\right]^2$$

Construction of T-X_{CO_2} Diagrams

The equilibrium T-X_{CO_2} curve can be accurately extrapolated from a narrow equilibrium bracket (± 10°C) obtained from experimental data using an integrated form of Eq. (d) (Greenwood, 1967a):

$$-\frac{1}{T_2} = A + \frac{R}{\Delta H_r}[n_{CO_2} \ln (X_{CO_2})_2 + n_{H_2O} \ln (X_{H_2O})_2], \quad \text{Eq. (f)}$$

where:

A = integration constant =

$$-\frac{1}{T_1} - \frac{R}{\Delta H_r}[n_{CO_2} \ln (X_{CO_2})_1 + n_{H_2O} \ln (X_{H_2O})_1],$$

which is evaluated at the starting point. Although the initial point for integration is usually taken as the midpoint of an equilibrium bracket (Fig. 3), the total temperature uncertainty of the bracket must be considered as a source of error in the extrapolation (*i.e.*, curves a and c in Figure 3). This means of extrapolating T-X equilibria is based on the assumption that ΔH_r is constant over the integration interval and that it is equal to the value obtained at the starting point $[T_1, (X_{CO_2})_1]$. The assumption of constant ΔH_r ($= T\Delta S_r$) is suspect for the following reasons: (1) ΔS_r varies with changing X_{CO_2} in the fluid, reflecting: $\bar{S}_i - S_i^0 = -R \ln a_i$, and (2) ΔS_r varies with temperature, primarily reflecting the large effect of temperature on molar entropy of fluid species. An exact extrapolation of the curve could be derived by the expression:

$$\Delta S_r = (\Delta S_r)_{T_1} + \int_{T_1}^{T_2} \frac{\Delta(Cp)_r}{T}\,dT - \int_{(X_{CO_2})_1}^{(X_{CO_2})_2} d(n_{CO_2} R \ln X_{CO_2}) - \int_{(X_{H_2O})_1}^{(X_{H_2O})_2} d(n_{H_2O} R \ln X_{H_2O}) \quad \text{Eq. (g)}$$

where $(X_{CO_2})_1$ and $(X_{H_2O})_1$ refer to the initial point of integration. Computer programs are available for exact solutions of the above expression[3]. In general, the loci of T-X equilibria extrapolated with constant ΔS_r are little different from those of the same reactions extrapolated with changing ΔS_r. Figure 4 shows T-X extrapolations of selected equilibria from the midpoints of experimental equilibrium brackets. At the scale of these diagrams, the solid curves, calculated with changing ΔS_r, are indistinguishable from those extrapolated with constant ΔS_r.

Variations in pressure can have profound effects on the T-X topologies of certain systems. If, for example, we restrict ourselves to an isocompositional plane in a P-T-X_{CO_2} diagram (*e.g.*, Fig. 1b), various mixed-volatile equilibria will have different slopes on this section, reflecting differences in ΔS_r and ΔV_r through the Clapeyron equation:

$$\left(\frac{dP}{dT}\right)_{X_{CO_2}} = \frac{\Delta S_r}{\Delta V_r}$$

The relative $(dP/dT)_{X_{CO_2}}$ slopes of various equilibria will thus determine changes in T-X topology with pressure. T-X locations of invariant points formed either by acutely intersecting equilibria, or by the intersection of solid-solid reactions with devolatilization equilibria, will in general be most sensitive to

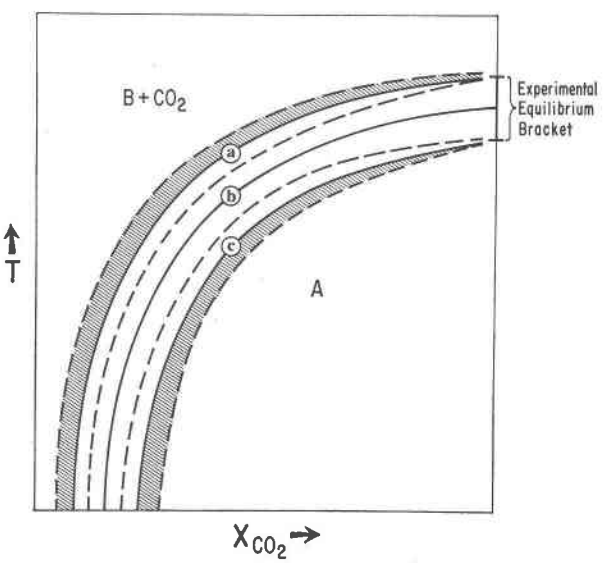

FIG. 3. Illustration of error analysis in T-X_{CO_2} equilibria extrapolated from an experimentally determined equilibrium bracket at $X_{CO_2} = 1$. Curves **a**, **b**, and **c** are extrapolated by calculating ΔS_r using the *average* entropy for all phases (as tabulated in thermochemical tables) from the top, middle, and bottom, respectively, of the equilibrium bracket. Dashed lines about **a** and **c** are calculated using the maximum and minimum values of ΔS_r from uncertainties in tabulated entropy values. The significance of hachured areas is explained in text.

[3] APL and Fortran programs for such calculations are in use at The Pennsylvania State University.

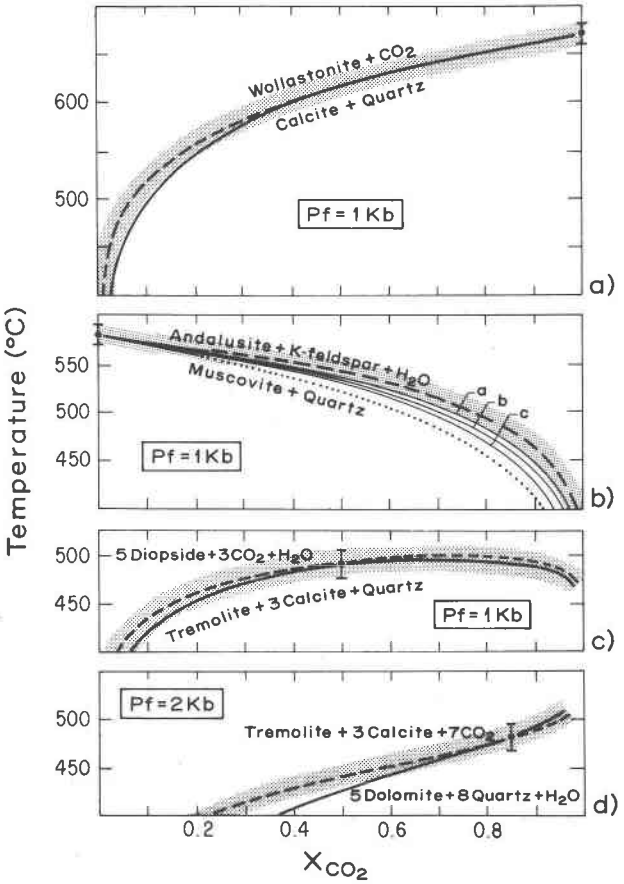

FIG. 4. T-X_{CO_2} plots of equilibria extrapolated from the midpoints of experimentally determined data. Sources for experimental reversals are: (a) Harker and Tuttle, 1956; (b) Althaus *et al* (1970); (c) and (d) Slaughter, Kerrick and Wall, 1974. Solid lines were calculated assuming ideal mixing in the fluid, and changing ΔS_r with temperature and X_{CO_2}. The dashed lines were extrapolated using CO_2 and H_2O activities (see text). Curves **a**, **b**, and **c** in Figure (b) are calculated assuming ideal mixing using the respective maximum, average, and minimum ΔS_{solids} from the data of Robie and Waldbaum (1968); dotted curve is for microcline whereas the other curves are for sanidine.

pressure changes. A striking example of topologic variation of T-X equilibria with changing pressure is discussed later [Fig. 13(b)–(d)].

T-X topologies involving several equilibria can be constructed following the rules of Schreinemakers. The theory behind derivation and placement of stable and metastable equilibria about each invariant point has been clearly outlined by Zen (1966). Invariant point analysis is straightforward for simple systems. However, for complex systems with equilibria involving many phases, especially those with large stoichiometric coefficients in the balanced reactions, invariant point analysis can be accomplished by matrix algebra. Computer programs have been written for these calculations (Finger and Burt, 1972).

Considerable progress can be made in graphical derivation of mixed-volatile equilibria with a minimum of good experimental data. With reliable equilibrium brackets on a few key equilibria in a particular system, the entire topology can be constructed with reasonable accuracy by extrapolations of equilibria based on calculation of ΔS_r [Eq. (f)]. Entropy data exists for many minerals of interest (Robie and Waldbaum, 1968); furthermore, entropy estimates can be made using additivity methods as originally outlined by Fyfe, Turner, and Verhoogen (1958), and carried out since by a number of investigators (*e.g.*, Newton, 1966; Zen, 1972). In making entropy estimates by additivity it is best to use appropriate additions of minerals (*e.g.*, Kerrick and Cotton, 1971, p. 363) rather than by adding simpler oxides as suggested by Fyfe, Turner, and Verhoogen (1958). Entropy estimates using minerals are better than those from oxides because the entropy correction from ΔV is smaller. Furthermore, additivity using hydrous phases of similar structure avoids the large error in the entropy of H_2O in using a simple oxide summation (Zen, 1972). Entropy data for H_2O has been derived over a wide range of temperature and pressure by Burnham, Holloway, and Davis (1969), whereas the entropy of CO_2 has been computed by Price (1955) and by Sharp (1962) from the P-V-T data of Kennedy (1954) for $P \leq 1.4$ kbar and T = 100°C-1000°C.[4] In deriving T-X topologies from

[4] The importance of knowing the *reference state* of a particular set of thermodynamic data cannot be overemphasized. Robie and Waldbaum present 1 atm. *third law* entropies for most phases, such that the entropy at a particular temperature has been derived by integration of the heat capacity equation ($S_T{}^{1\ atm} = \int_0^T Cp/T\ dT$), assuming the entropy is zero at 0°K. For some phases, such as alkali feldspars, they have added residual entropy term to correct for Al/Si disorder. Burnham, Holloway, and Davis (1969) present entropy of H_2O with the triple point as a base (P = 0.0061 bar, T = 0.01°C), whereas the tables of Price (1955) are entropy differences of CO_2 between T and 0°C. Thus, to calculate ΔS_r in terms of third law entropies (as is commonly done), 15.130 cal/mol ($= \int_0^{273.01} (Cp)_{H_2O}/T\ dT$) must be added to the data of Table 3 in Burnham, Holloway, and Davis (1969) whereas 50.31 ($= \int_0^{273} (Cp)_{CO_2}/T\ dT$) must be added to the entropy data of Price (1955). Sharp (1962) presents thermodynamic data for CO_2 with a reference state of 0°K.

experimental brackets, one should consider the error stemming from uncertainty in the entropy data of phases. The uncertainty in thermochemical data as tabulated by Robie and Waldbaum (1968) has a *statistical* base, and it is derived from two standard deviations from the mean of replicate calorimetric measurements. The entropy uncertainty given by Robie and Waldbaum (1968) applies to 25°C. Significance of the entropy uncertainty on a schematic *T-X* extrapolation is given in Figure 3. Because the data derived from calorimetric measurements has a statistical base, a calculated ΔS_r based on tabulated (average) entropies is more probable than the extreme values of ΔS_r derived by uncertainties in the entropy data. Thus, it is less probable that the extrapolated reaction lies in the hachured area of Figure 3 than between curves a and c. Extrapolations of all reactions in Figure 4 were carried out assuming ideal mixing in the fluid, and using the entropy uncertainties given by Robie and Waldbaum (1968). Entropy uncertainties are insignificant in all extrapolations except for that shown in Figure 4b, reflecting the relatively large uncertainty in the entropy of sanidine. Once a reaction has been extrapolated from an experimental reversal (or reversals), the topology can be constructed by intersection with other extrapolated equilibria. From these intersections, additional equilibria are derived from Schreinemakers analysis and are extrapolated with entropy data using equation (f).

Another method of deriving *T-X* equilibria can be referred to as the "free energy coupling method" as outlined by Slaughter, Kerrick, and Wall (1974). This involves setting $\Delta G_r = 0$ for a particular reaction within an experimental equilibrium bracket, deriving other reactions by the appropriate coupling with the experimentally determined equilibrium, and calculating the equilibrium *T-X* curves of the derived reactions where $\Delta G_r = 0$, by computer calculations involving published and estimated entropies for solids, and free energy data for H_2O and CO_2. This procedure avoids large errors resulting from free energy calculations based on ΔH_f (free energy of formation) data.

T-X equilibria can also be derived from equilibrium constants as outlined by Eugster and Skippen (1967), and by Skippen (1971). Skippen (1971) derived equilibrium constants for five key reactions in the system: $CaO\text{-}MgO\text{-}SiO_2\text{-}H_2O\text{-}CO_2$, as determined from log *K vs* $1/T$ plots of experimental data, such as shown in Figure 5a. He computed equilibrium

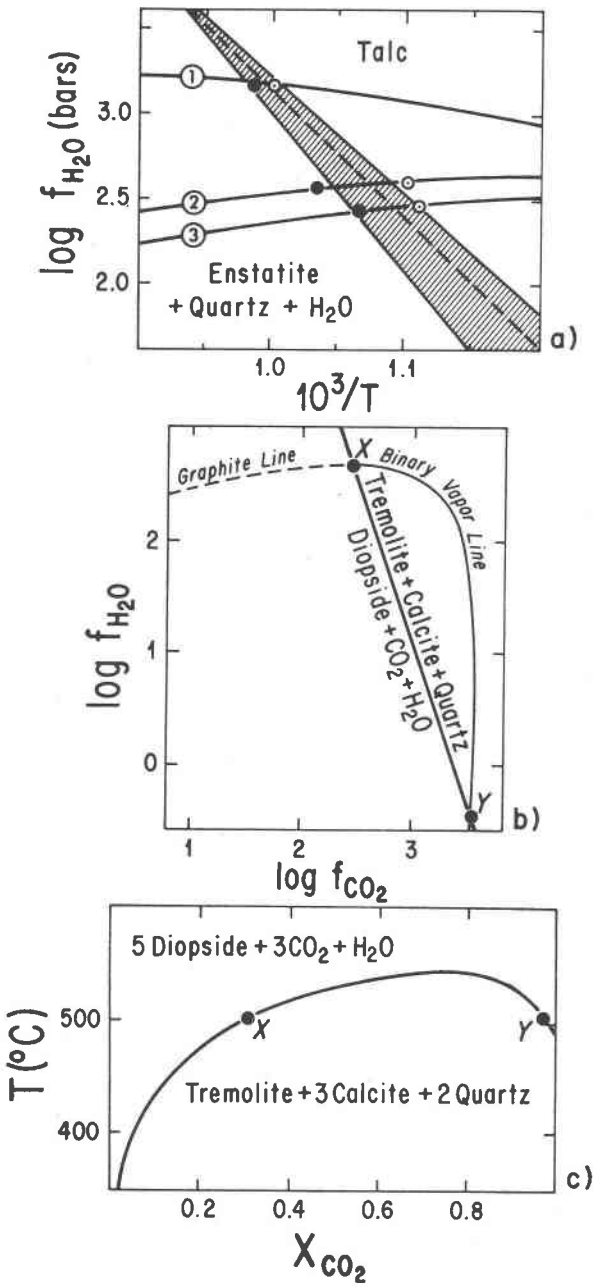

FIG. 5. (a) Log *K vs* $1/T$ plot taken from Skippen (1971). Curves (1)–(3) are for different oxygen buffers. Open circles represent runs with growth of talc, whereas closed circles are runs involving talc breakdown. Dashed line is equilibrium line chosen by Skippen (1971); the hachured area represents the total error band of the equilibrium boundary. (b) Plot of log f_{H_2O} *vs* log f_{CO_2} taken from Skippen (1971). Points **X** and **Y** are also shown in Figure 5c. (c) $T\text{-}X_{CO_2}$ diagram at $P_f = 2$ kbar showing points **X** and **Y** calculated from Figure 5b.

constants for 44 other reactions in this system by appropriate coupling with the five basic reactions. For a mixed-volatile reaction involving pure solid phases (*i.e.*, no solid solution, such that the activities of solids are unity), the equilibrium constant can be expressed in terms of fugacities of gas species; thus, for example, for the reaction: tremolite + 3 calcite + 2 quartz = 5 diopside + 3 CO_2 + H_2O we have:

$$K = f_{CO_2}{}^3 \cdot f_{H_2O}$$

Skippen's equilibrium constants were derived for a total pressure of 2 kbar; thus in the last column of Skippen's Table 10, a constant is given (= $\Delta V_{solids}/2.303\ R$) for each reaction to correct the equilibrium constant to pressures other than 2 kbar. Each reaction can be plotted on a $\log f_{H_2O} - \log f_{CO_2}$ diagram such as shown in Figure 5b.[5] Intersection of the equilibrium boundary with the line for a binary H_2O-CO_2 fluid (the "binary vapor line") gives the equilibrium fugacities of CO_2 and H_2O in the presence of a H_2O-rich fluid (point **X**) and with a CO_2-rich fluid (point **Y**). X_{CO_2} at points **X** and **Y** are calculated from:

$$(X_{CO_2})_{P,T} = \frac{f_{CO_2}{}^*}{f_{CO_2}{}^0}$$

This data is then translated to the *T-X* diagram (Figure 5c), and a similar procedure at the same fluid pressure and various temperatures allows construction of the *T-X* curve for this reaction. A Fortran computer program is available for these calculations (Skippen, 1970). It should be noted that since the equilibrium constants have been based solely on experimental data, this procedure avoids the typically inaccurate calculation of equilibrium constants taken from tabulated thermochemical data, these latter inaccuracies mostly resulting from uncertainty in ΔH_f as determined from measurements of heats of solution.

Barron (1974) has outlined a graphical method of extrapolating *T-X* equilibria.

The self-consistency of *P-T-X*$_{CO_2}$ equilibria must be considered when evaluating experimental data. Since a few key equilibria can generate all possible reactions within a system (*e.g.*, Skippen, 1971, 1974), self-consistency tests must be carried out either by Schreinemakers analysis of stable and metastable equilibria (Zen, 1966) or by extrapolations with thermochemical data (Skippen, 1974; Slaughter, Kerrick, and Wall, 1974). A *necessary* test for self-consistency is that all possible independent combinations and extrapolations of reactions will generate equilibria which pass through their experimentally determined equilibrium bracket(s). The "free energy coupling" method described by Slaughter, Kerrick, and Wall (1974) provides a very useful technique in this regard, as it permits independent checks on the location of equilibria within *P-T-X*$_{CO_2}$ space. An alternative approach to experimental self-consistency is to examine thermodynamic data derived from experimental equilibrium brackets (Zen, 1972; Gordon, 1973).

Non-Ideal Mixing

For improved accuracy in constructing *T-X* diagrams we must consider the consequences of non-ideal mixing in the fluid. Using available *P-V-T* data, Ryzhenko and Malinin (1971) computed fugacity coefficients at T = 400–750°C and P = 400–2000 bars for H_2O-CO_2 mixtures, and for other gas mixtures. Greenwood's (1973) data, calculated from his *P-V-T* measurements at P = 1–500 bars, and T = 450–800°C, shows positive deviations from ideal mixing for both H_2O and CO_2, in agreement with the data of Ryzhenko and Malinin (1971); at a fixed pressure the deviation increases with decreasing temperature. C. Wayne Burnham and co-workers at The Pennsylvania State University are experimentally determining the thermodynamic properties of H_2O-CO_2 mixtures to higher pressures. As expected, mixtures of H_2O and CO_2 become more ideal in going toward lower pressure and/or higher temperature. In the low temperature range, non-ideality becomes so marked that, below a certain temperature, H_2O and CO_2 separate into two phases, the large positive activity coefficients of H_2O and CO_2 at low temperature causing ΔG_{mix} (= $X_{H_2O}\ RT \ln a_{H_2O}$ + $X_{CO_2}\ RT \ln a_{CO_2}$) to be positive.

Non-ideal mixing can be accounted for in a modified form of Eq. (f):

$$-\frac{1}{T_2} = B + \frac{R}{\Delta H_r}\left[n_{CO_2} \ln (X_{CO_2})_2 + n_{H_2O} \ln (X_{H_2O})_2\right]$$

$$+ \frac{R}{\Delta H_r}\left[n_{CO_2} \ln (\gamma_{CO_2})_2 + n_{H_2O} \ln (\gamma_{H_2O})_2\right] \quad \text{Eq. (h)}$$

where:

$$B = A - \frac{R}{\Delta H_r}\left[n_{CO_2} \ln (\gamma_{CO_2})_1 + n_{H_2O} \ln (\gamma_{H_2O})_1\right],$$

[5] This type of plot will be discussed in more detail in the section on μ–μ diagrams.

which is evaluated at the initial point of integration, and where:

A = integration constant in Eq. (f).

The effect of non-ideality on extrapolated mixed-volatile equilibria is schematically shown in Figure 6. As an example, consider reaction ⟨2⟩ at a fixed value of X_{CO_2}. Because of the positive term involving activity coefficients in Eq. (h), the equilibrium temperature will be higher than that for the same X_{CO_2} with ideal mixing [Eq. (f)]. These arguments also hold for the relative locations of the ideal *vs* non-ideal curves for equilibria ⟨3⟩ and ⟨4⟩. The progressive divergence of ideal *vs* non-ideal curves for equilibria ⟨2⟩, ⟨3⟩, and ⟨4⟩ in going toward lower temperature reflects the combined effects of: (a) the marked non-ideal mixing of a gaseous species (H_2O or CO_2) where the mole fraction of this species is between 0 and 0.5 (see, for example, Greenwood, 1973, Fig. 1); and (b) increasing non-ideality of mixing toward lower temperature. Comparison of the ideal *vs* non-ideal curves for type ⟨5⟩ equilibria is more complex. Where $|n_{CO_2}| > |n_{H_2O}|$ (⟨5″⟩ reactions) or $|n_{CO_2}| < |n_{H_2O}|$ (⟨5′⟩ reactions) the relative locations of the ideal *vs* non-ideal curves will be as shown in Figure 6. This conclusion is evident from Eq. (h). However, with $|n_{H_2O}| = |n_{CO_2}|$ the relative locations of the extrapolated ideal *vs* non-ideal curves is not apparent from inspection of Eq. (h). Examples of activity-corrected extrapolations of equilibria are shown as dashed lines in Figure 4. These corrections were accomplished with a computer program using the procedure outlined by Slaughter, Kerrick, and Wall (1974). It is clear that correction for non-ideal mixing is important, especially in long extrapolations. Errors in topologies resulting from neglecting non-ideal mixing in the fluid will be most serious at low temperatures where (a) invariant points are derived by long extrapolations of equilibria, and (b) invariant points are formed by reactions intersecting at small angles.

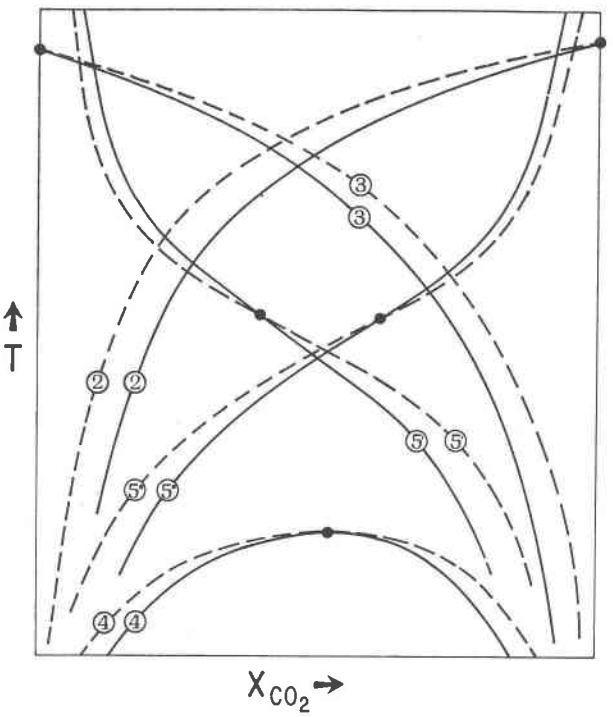

FIG. 6. Comparison of various types of mixed-volatile equilibria for ideal (solid lines) *vs* non-ideal (dashed lines) mixing in vapor phase. Solid circles represent equilibrium points from which the "non-ideal" and "ideal" curves were extrapolated.

Non-Binary Fluid Mixtures in the System C-O-H

So far we have considered strictly binary H_2O-CO_2 mixtures in the vapor phase. However, the fluid in many metamorphic systems, especially those containing graphite, may deviate considerably from a binary mixture. Significant amounts of reduced gas species (*e.g.*, CO and CH_4) occur in a C-O-H fluid in equilibrium with graphite at low f_{O_2}. The proportion of gaseous species can be derived by solution of simultaneous equations of the equilibrium constants for the reactions:

(1) graphite + O_2 = CO_2
(2) graphite + 1/2 O_2 = CO
(3) graphite + 2 H_2 = CH_4
(4) H_2 + 1/2 O_2 = H_2O

coupled with the additional expression:

$$(5)\quad P_{fluid} = P_{CO_2} + P_{CO} + P_{CH_4} + P_{H_2O} + P_{H_2} = \frac{f_{CO_2}}{\gamma_{CO_2}} + \frac{f_{CO}}{\gamma_{CO}} + \frac{f_{CH_4}}{\gamma_{CH_4}} + \frac{f_{H_2O}}{\gamma_{H_2O}} + \frac{f_{H_2}}{\gamma_{H_2}}$$

Each calculation is made at fixed P_{fluid} ($= P_{solid}$), T, and f_{O_2} [following the phase rule: $F = C - P + 2$, in a 3-component C-O-H system containing two phases (graphite + fluid), the system is completely defined by specifying three independent variables]. The foregoing rather extensive calculations, more completely developed by French[6] (1966, p. 227–228),

[6] Inaccuracy in French's (1966) computations stems from the fact that he neglected: (a) fugacity coefficients of all gas species, and (b) the pressure effect on the equilibrium constants of reactions involving graphite.

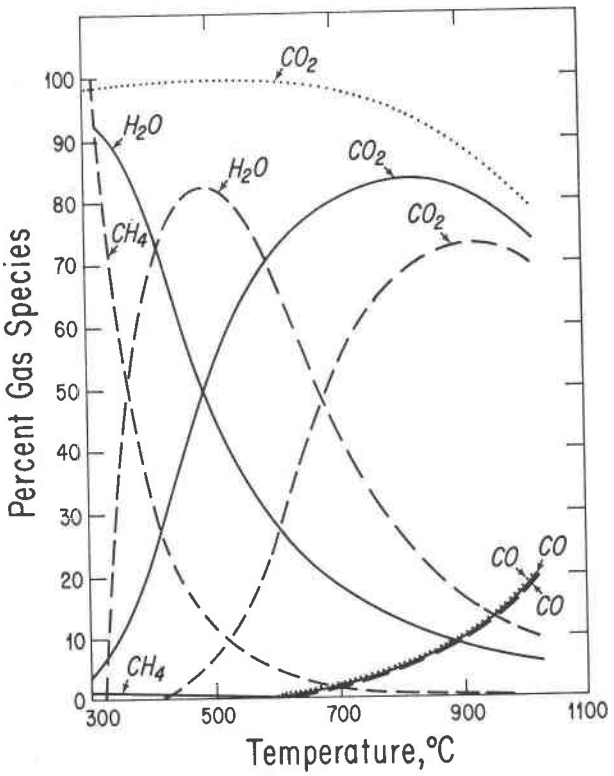

FIG. 7. Composition of a C-O-H gas at 2 kbar in the presence of graphite (from Eugster and Skippen, 1967). Dotted, solid, and dashed curves are for the HM, NNO, and QFM buffers, respectively.

may now be accomplished with computer programs.[7] Such calculations have been made by Eugster and Skippen (1967) on the proportion of gaseous species in the C-O-H system (Fig. 7) but contain errors because (a) the computations assumed ideal mixing in the fluid (*i.e.*, fugacity coefficients for the *pure* gaseous species were used), and (b) fugacity coefficinets for CO and CH_4 were taken from reduced variable plots (reproduced in Garrels and Christ, 1965, p. 25). Use of data from a recent compilation of fugacity coefficients by Ryzhenko and Volkov (1971) would undoubtedly lead to improved accuracy in these calculations.

The effect of non-binary fluids on *T-X* equilibria can be explained with the aid of Figure 8a. Change in fluid composition in going from the front H_2O-CO_2 surface is similar to the change in fluid composition that would be produced in a graphite-bearing system with progressive reduction in f_{O_2}. As shown in Figure 8b, progressive increase in CH_4 reduces the stability field of the hydrous phase. On a *T-X* diagram, equilibria of types ⟨3⟩ and ⟨4⟩ are similarly affected. However, the effect of CH_4 addition on *T-X* projections of type ⟨5⟩ equilibria is somewhat more complex. For example, for the equilibrium (Fig. 8c), 3 dolomite + 4 quartz + H_2O = talc + 3 calcite + 3 CO_2,

$$K = \frac{a_{Tc} \cdot (a_{Cc})^3 \cdot (a_{CO_2})^3}{(a_{Do})^3 \cdot (a_Q)^4 \cdot a_{H_2O}} = \left[\frac{(X_{CO_2})^3}{X_{H_2O}}\right]_{ideal}$$

For the binary H_2O-CO_2 system at $X_{CO_2} = X_{H_2O} = 0.5$ (point A in Fig. 8c)

$$K = \frac{0.5^3}{0.5} = 0.25$$

If CH_4 is added to the point where $X_{CO_2} = 0.4$:

$$K = 0.25 = \frac{(0.4)^3}{X_{H_2O}}$$

Thus,

$$X_{H_2O} = 0.256$$

Recalculation so that $X_{H_2O} + X_{CO_2} = 1$ yields

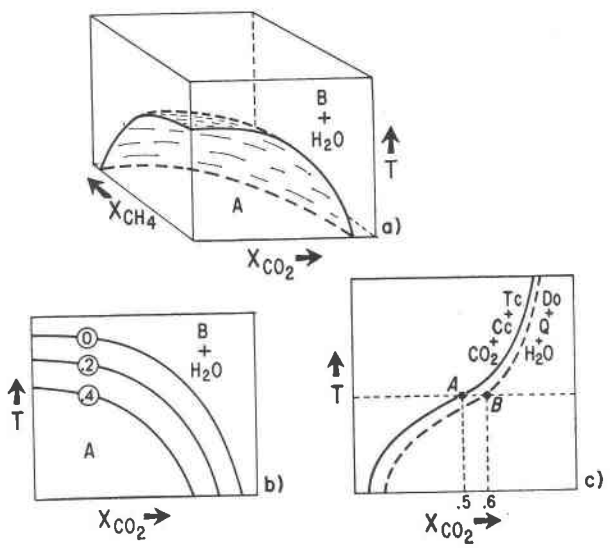

FIG. 8. (a) Schematic T-X_{CO_2}-X_{CH_4} diagram showing the equilibrium surface for a reaction. (b) T-X_{CO_2} projection showing curves of constant X_{CH_4} (circled). (c) Effect of CH_4 on a type ⟨5⟩ mixed-volatile reaction. Point **A** and solid curve are for a binary H_2O-CO_2 fluid, whereas point **B** and dashed curve are projections from a CH_4-bearing system.

[7] A Fortran program for these calculations is available through G. Skippen of Carleton University; H. Ohmoto of the Pennsylvania State University has developed an APL program for these calculations.

$X_{CO_2}^* = 0.61$ and $X_{H_2O}^* = 0.39$.[8] Thus, the *T-X projection* of this reaction shifts to the right with progressive addition of CH_4. By the same line of reasoning as above, T-X_{CO_2} projections of type ⟨5⟩ equilibria with $|n_{H_2O}| > |n_{CO_2}|$ will shift to the left with increasing proportion of CH_4 in the fluid, whereas reactions with $|n_{H_2O}| = |n_{CO_2}|$ will be unaffected. Non-ideal mixing would, of course, complicate these arguments. It is important to note that in a system at equilibrium the proportion of methane is not an independent variable, as could be falsely conveyed by Figure 8. In a system buffered with oxygen the proportion of methane is a complex function of temperature (Figure 7), whereas in an unbuffered system the proportion of methane is controlled by homogeneous equilibria in the gas phase (*e.g.*, $2\ H_2O + CH_4 = CO_2 + 4\ H_2$). Hence, a T-X projection for a reaction boundary would not follow an isocompositional projection as in Figure 8b.

$\mu_{H_2O} - \mu_{CO_2}$ *Diagrams*

The role of mixed-volatiles in subsolidus equilibria can be illustrated not only with T-X plots but also with P-X_{CO_2} and P-T projections (Fig. 1)—or by plotting either log f_{H_2O} *vs* log f_{CO_2} (Skippen, 1971) or μ_{H_2O} *vs* μ_{CO_2} (Korzhinskii, 1959; Zen, 1961; Burt, 1971, 1972b; Finger and Burt, 1972; Watts, 1973). These last two types of diagrams are in essence equivalent since the chemical potential and fugacity of a gas species can be related by:

$$(\mu_i)_T^P = \mu_i^0 + RT \ln f_i$$

Thus, changes in μ_i are directly related to changes in f_i. The thermodynamic basis for a mixed-volatile reaction on a $\mu_{H_2O} - \mu_{CO_2}$ diagram can be derived from Eq. (e), which at constant temperature yields:

$$n_{H_2O}\, d\mu_{H_2O} + n_{CO_2}\, d\mu_{CO_2} = 0$$

The expression can be related to reactions ⟨1⟩–⟨5⟩ by noting that $n_{H_2O} = 0$ in ⟨2⟩, $n_{CO_2} = 0$ in ⟨3⟩, n_{CO_2} and n_{H_2O} have the same sign in ⟨4⟩ (since they occur on the same side of the reaction), whereas in reaction ⟨5⟩, n_{CO_2} is opposite in sign to n_{H_2O} when the reaction is written with both volatiles on the same side. Assuming fixed water contents of hydrous phases, all mixed-volatile reactions will plot as straight lines with slopes given as:

[8] We define X_{CO_2} as: $N_{CO_2}/(N_{CO_2} + N_{H_2O} + N_{CH_4})$, and $X_{CO_2}^* = N_{CO_2}/(N_{CO_2} + N_{H_2O})$ in the ternary fluid.

TABLE 1. Slope Calculations for Equilibria on μ_{H_2O}–μ_{CO_2} Diagrams

Reaction	Slope
Dolomite + 2 Quartz = Diopside + $2CO_2$	$\frac{d\mu_{H_2O}}{d\mu_{CO_2}} = -\frac{2}{0} = -\infty$
3 Dolomite + 4 Quartz + H_2O = Talc + 3 Calcite + $3CO_2$	$\frac{d\mu_{H_2O}}{d\mu_{CO_2}} = \frac{3}{1} = +3$
Tremolite + 3 Calcite + 2 Quartz = 5 Diopside + $3CO_2$ + H_2O	$\frac{d\mu_{H_2O}}{d\mu_{CO_2}} = -\frac{3}{1} = -3$
Tremolite + 3 Calcite = 4 Diopside + Dolomite + CO_2 + H_2O	$\frac{d\mu_{H_2O}}{d\mu_{CO_2}} = -\frac{1}{1} = -1$

$$\frac{d\mu_{H_2O}}{d\mu_{CO_2}} = -\frac{n_{CO_2}}{n_{H_2O}} \qquad \text{Eq. (i)}$$

Examples of slope calculations of representative equilibria in calcareous systems are given in Table 1; these and other related reactions are shown in a $\mu_{H_2O} - \mu_{CO_2}$ diagram (Fig. 9a). Eq. (i) indicates that only type ⟨5⟩ equilibria will have positive slopes on $\mu_{H_2O} - \mu_{CO_2}$ diagrams. It is important to emphasize that for equilibria on these diagrams, μ_{H_2O} and μ_{CO_2} are independent of one another; therefore, H_2O and CO_2 are "boundary value components" in the terminology of Zen (1963). Considering systems at fixed P_f (= P_s) and T, and with H_2O and CO_2 as the only "volatile" components, a $\mu_{H_2O} - \mu_{CO_2}$ diagram for the most part reflects totally condensed (vapor-absent) conditions. This is evident by considering an isothermal line on a T-X_{CO_2} section (*e.g.*, in Fig. 9b), and translating this to the $\mu_{H_2O} - \mu_{CO_2}$ diagram (Fig. 9a). At any point along the resultant curved line (here referred to as the "binary vapor line"), $P_{H_2O} + P_{CO_2} = P_{fluid}$. Points **X**, **Y**, and **Z** in Figure 9a are analogous to those shown in Figure 9b. Topologic similarities between the T-X_{CO_2} diagram and the $\mu_{H_2O} - \mu_{CO_2}$ diagram are evident. Because μ_i is a logarithmic function of f_i, the flat portion of the vapor saturation line at high μ_{H_2O} corresponds to the very low X_{CO_2} range, whereas the subvertical portion represents very high X_{CO_2}. At a fixed P-T condition the region on the convex side of the vapor saturation line is unattainable with $P_f = P_s$ because the chemical potentials of H_2O and CO_2 along the binary vapor line represent the maximum attainable values. Thus, the region on the convex side can be reached by lowering temperature and/or raising pressure.

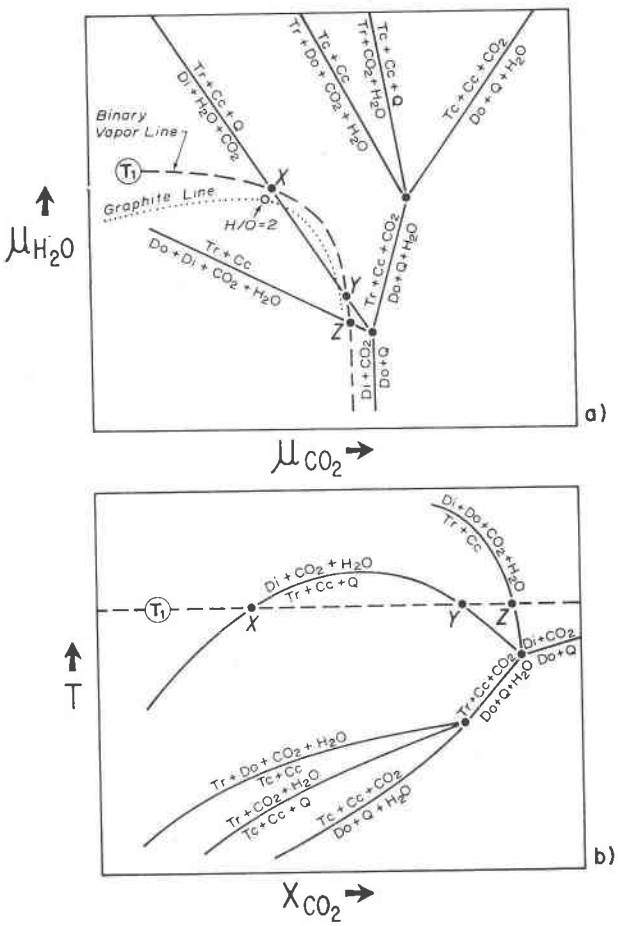

FIG. 9. (a) Schematic μ_{H_2O}-μ_{CO_2} diagram showing some equilibria in the system CaO-MgO-SiO_2-CO_2-H_2O. Isotemperature binary vapor line, and points **X**, **Y**, **Z**, are also shown on Figure 9b. Dotted graphite line is for temperature T_1. (b) Schematic T-X_{CO_2} diagram showing the same equilibria as in Figure 9a.

In the presence of graphite, the vapor line is located on the concave side of that for the binary H_2O-CO_2 system (Skippen, 1971), since addition of other gas species to a CO_2-H_2O fluid at a fixed P and T will lower f_{CO_2} and f_{H_2O} (and, thus, μ_{CO_2} and μ_{H_2O}). The graphite line is closer to the binary vapor line in the presence of high μ_{CO_2} than in the high μ_{H_2O} region. As shown in the diagrams of French (1966, p. 230), this reflects the fact that CH_4 is less abundant in fluids with a high CO_2/H_2O ratio (high f_{O_2}) than in those with a low CO_2/H_2O ratio (low f_{O_2}). In following the graphite line toward more CO_2-rich compositions, f_{O_2} in the vapor increases; eventually the point is reached where graphite becomes unstable. Termination of the graphite line at high μ_{CO_2} is shown in Figure 9a.

Advantages of $\mu_{H_2O} - \mu_{CO_2}$ diagrams over T-X plots include:

(a) Equilibria plot as straight lines whose slopes are easily computed,
(b) Vapor-deficient systems can be investigated.
(c) The extremal regions of X_{CO_2}, within which numerous invariant points may be crowded on a T-X diagram, are expanded on a $\mu_{H_2O} - \mu_{CO_2}$ diagram (Finger and Burt, 1972).

It must be stressed that a $\mu_{H_2O} - \mu_{CO_2}$ diagram is both *isobaric* and *isothermal*; thus their utility in metamorphic studies lies in the analysis of the variation in the chemical potentials of volatile components within relatively small domains within which P_{total} and T are constant.

An additional complexity regarding non-binary fluid compositions at elevated pressures and temperatures stems from the solution of solids in the fluid phase. However, the small proportion of dissolved solids in fluids in the metamorphic P-T range will have a negligible effect in reducing the activities of gas components compared to that of pure fluids without dissolved minerals. For example, from the data of Anderson and Burnham (1965) on quartz solubility, $X_{H_2O} \geq 0.97$ for $P \leq 8$ kbar and $T \leq 900$°C. Furthermore, the solubility of quartz exponentially decreases with increasing X_{CO_2} (Shettel, 1973).

Fluids Not in the System C-O-H

Thus far we have considered only fluids in the C-O-H system. However, because sulfides are common accessories in metamorphic rocks, consideration of the system C-O-H-S seems necessary. Morgan (1970), for example, has calculated significant proportions of H_2S in fluids with the assemblage: graphite-pyrite-pyrrhotite, at moderate temperature (~525°C) and high pressure (~7 kbar) conditions. Similar calculations were made by Guidotti (1970). In certain rock systems it is necessary to consider other species in the vapor phase. For example, in the presence of fluorine-bearing phases the system C-O-H-F would be appropriate; calculation of the proportion of vapor phase species in this system is outlined by Munoz and Eugster (1969). Burt (1972c) derived numerous equilibria involving F and CO_2 in the system Ca-Fe-Si-C-O-F. Holloway and Reese (1974) calculated fluid compositions in the system C-O-H-N, of use in the study of systems with $P_{H_2O} + P_{CO_2} < P_{fluid}$.

Experimental Techniques

The strengths and weaknesses of experimental techniques used in studying mixed-volatile equilibria will now be discussed.

Greenwood (1961)[9] illustrates the experimental apparatus used by him to study mixed-volatile equilibria (Greenwood, 1967a, 1967b; Gordon and Greenwood, 1970, 1971). His experimental technique usually provides convincing evidence of reaction reversibility since, on either side of an equilibrium, the stable assemblage (as verified by optical and X-ray analysis) has spontaneously nucleated and grown at the expense of the unstable assemblage (*i.e.*, no seeds of the stable assemblage were added to the starting mix). Extensive reaction is unnecessary with this method, since small amounts of newly nucleated material can be determined optically. This technique could be plagued by a small amount of back-reaction during quench in runs starting with the high temperature assemblage. However, the consistent results of Greenwood's runs on both sides of a proposed equilibrium boundary suggest that this problem is not significant in the reactions he has investigated. Greenwood's experiments are carried out with unsealed capsules in large-volume (25 cc) Morey bombs filled with H_2O and CO_2. This technique has the advantage of maintaining a constant vapor composition (*i.e.*, the reaction taking place has a negligible effect on the relatively large mass of volatiles in the system), but it has the disadvantage of introducing a potentially large difference in temperature between the recording thermocouple (placed in a well in the exterior of the vessel) and the capsules within the vessel (Boettcher and Kerrick, 1971). Thus, temperatures recorded by Greenwood *may* be higher than those of the sample capsules. At the termination of a run, the fluid is passed through a cold trap, where the amount of H_2O is determined by weighing, and the amount of other gases (mainly CO_2) are determined volumetrically. Thus, the gas compositions in Greenwood's experiments are *very* accurately known.[10] Through gas chromatography, Greenwood found negligible proportions of species other than H_2O and CO_2 in the vapor phase.

Experimentalists associated with the University of Göttingen determine reaction direction of mixed-volatile equilibria by monitoring changes in the vapor phase composition during experiments. All solid phases of the reaction are present throughout their runs. Since the recording thermocouple is placed adjacent to the capsules within the vessel, temperatures reported by the Göttingen experimentalists are probably very accurate. Experiments are carried out in sealed capsules, and the composition of the vapor phase is determined by the method outlined by Johannes (1969, p. 1085). With this technique the proportion of CO_2 in a capsule is determined by measuring the weight loss upon puncturing, whereas the amount of H_2O is determined by measuring the weight loss of the capsule upon drying at 110°C. During runs the capsules are buffered at or near Ni-NiO by the bomb wall (Huebner, 1971, p. 130), such that the fluid phase is essentially a binary H_2O-CO_2 mixture (see Fig. 7). Thus, it is safe to assume that the gas released upon puncturing the capsule is mostly CO_2. The main source of uncertainty in the determination of X_{CO_2} by this method stems from the possibility that some H_2O can escape with gaseous CO_2 upon puncturing a capsule. Because of this factor, calculated X_{CO_2} will be higher than the actual value. With fluid compositions of $X_{CO_2} = 0.5$ (produced from the decomposition of oxalic acid) this method is accurate to $\pm$ 2 mole percent (Kerrick 1972; Gordon and Greenwood, 1971). However, in more H_2O-rich fluids (especially with $X_{CO_2} = 0$-0.1) escape of H_2O along with CO_2 becomes a more serious problem, such that X_{CO_2} is accurate to perhaps $\pm$ 4 mole percent. In runs with a carbonate phase, Metz (1970) has independently determined the vapor composition by determining the amount of carbonate consumed or formed, through comparison of titration analyses of solutions of carbonates dissolved from run products with those from the starting mix. Metz (1970, p. 230) claims agreement between the two methods of determining the vapor composition. In many cases, the Göttingen experimentalists have attempted to obtain reaction reversal by approaching the equilibrium curve from both sides. The technique used in many of their experiments is illustrated in Figure 10. Experiments with several capsules containing identical starting mixtures are run in the same bomb at a fixed temperature, and the run is quenched after a fixed time, and one capsule is removed and analyzed for its vapor composition (capsule (1) in Figure 10). The remaining capsules are again subjected to the same *P-T* condition and the above process is repeated until the vapor composition

[9] A modification in the gas analysis system is outlined by Greenwood (1967b).

[10] Maximum error in gas analysis is stated as $\pm$ 0.30 percent (Greenwood, 1967a).

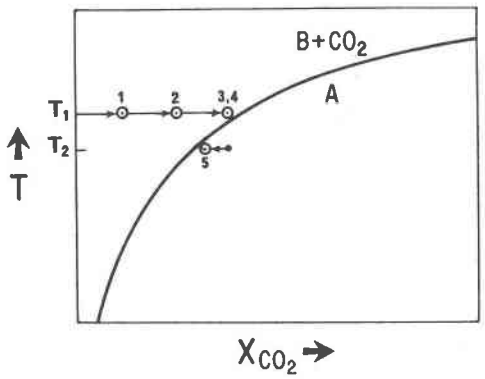

FIG. 10. Schematic illustration of experimental technique used by some investigators associated with the University of Göttingen. Numbers refer to capsules analyzed at successive stages of an experiment (see text). All capsules started with pure H_2O ($X_{CO_2} = 0$).

does not change (*e.g.*, *cf* capsules (3) and (4) in Figure 10). The remaining capsules are then run at a lower temperature (T_2), and the vapor composition is measured at the end of the run. Reaction reversal is claimed where the vapor composition (*e.g.*, capsule (5) in Figure 10) has migrated back from that of capsules (3) and (4). Providing that the fluid composition of the last capsule (#5) is distinctly more H_2O-rich than that at the end of the runs at T_1, this technique should be valid. However, in some cases, such as in the experiments of Metz, it is difficult to determine the history of capsules showing the critical back-reaction. Since such "critical" reversal points are few (see, for example, Figure 6 of Metz, 1970, p. 235), the previous temperature of this capsule (*i.e.*, T_1 in Figure 10) becomes critical. In essence, the potential difficulty is that the final X_{CO_2} of the "reversal" run *may* not be significantly different from X_{CO_2} at the end of the runs at higher temperature. However, Storre and Nitsch (1972) have used a somewhat different technique, whereby reaction reversal appears to have been demonstrated by monitoring significant changes in X_{CO_2} from *both sides* of the equilibrium boundary.

At The Pennsylvania State University we have used a number of independent methods to study mixed-volatile equilibria. Fluid compositions of $X_{CO_2} = 0.5$ are generated within sealed capsules by breakdown of oxalic acid (Holloway, Burnham, and Millhollen, 1968), whereas other values of X_{CO_2} are obtained with a mixture of silver oxalate (which breaks down to Ag + CO_2 at about 100°C) and liquid H_2O. Much of our work involves determination of reaction direction by monitoring weight changes of single crystals of one of the reaction phases (*e.g.*, Kerrick, 1968, 1972). This method is not suitable for minerals with well-developed cleavages and has so far been used with single crystals of quartz (Kerrick, 1968, 1972; A. B. Thompson, 1970), corundum (Evans, 1965; Haas, 1972, Holdaway, 1972), andalusite (Kerrick, 1968; Holdaway, 1971), adularia (Evans, 1965), and mullite (Evans, 1965). Numerous studies have shown that minor amounts of impurities adhering to the surface of the single crystals do not introduce a significant error where weight changes are more than about 20 μg. This technique is an extremely sensitive indicator of reaction direction, as very little reaction is necessary to cause significant weight changes of the single crystal. Since only one of the phases participating in the desired reaction is monitored, ambiguity can arise as to the reaction causing the weight change of the single crystal. Because little reaction occurs, small amounts of unwanted phases could nucleate, but be overlooked in X-ray or optical examination of the run product. Thus, interpretation of single crystal studies should be checked by independent methods. In addition to single crystal runs, we have used combinations of:

(a) Long runs with all-powdered starting materials followed by X-ray analysis (Kerrick, 1968, 1972; Slaughter, Kerrick, and Wall, 1974).
(b) Examination of the charge by scanning electron microscopy (Haas, 1972).
(c) Monitoring reaction direction by following changes in fluid composition during runs (Kerrick, Hunt, and Wall, 1973).
(d) Determination of reaction direction in runs with calcite by analysis of the amount of calcite consumed or formed (Slaughter, Kerrick, and Wall, 1974).

In equilibria examined to date, data from single crystal runs are compatible with that obtained by independent methods.

Investigators associated with the Johns Hopkins University have developed a "solid phase buffer technique" for investigating mixed-volatile equilibria (Eugster and Skippen, 1967; Skippen, 1971). Huebner (1971) presents a summary of this experimental method. The capsule arrangement during runs is illustrated in Figure 11. The C-O-H fluid, which is generated by an initial mixture of oxalic acid, benzoic acid, and liquid water, permeates the unsealed inner

capsule during the run. The oxygen buffer in the outer capsule imposes a fixed f_{H_2} on the inner fluid by diffusion of hydrogen through the intermediate platinum tube. The composition of the fluid in equilibrium with graphite at a fixed P_f, T, and f_{H_2} is calculated as outlined previously. Reaction direction is determined by optical and X-ray examination of run products. Inherent in the solid phase buffering technique is the assumption of equilibrium between the solids and fluids. It is possible that, because of sluggish reaction kinetics of the buffer and/or slow diffusion of hydrogen through platinum, equilibrium is not achieved. As discussed previously, a complication arises from the errors in the calculated gas compositions in graphite-bearing systems. However, the consistency in the results of Skippen (1971) for a particular reaction in comparing one buffer to the next (see, for example, Fig. 5 of Skippen, 1971), lends credence to his assumption of equilibrium fugacities in the fluid. For the most part, Skippen (1971) has been very careful in his interpretation of reaction direction, doing so only for runs where there has been extensive reaction. However, in some cases he has decided upon reaction direction where little reaction has occurred (see, for example, Table 6 of Skippen, 1971). A general point to be made here is that in evaluating the validity of reversals in seeded runs based on relatively insensitive techniques, such as the all-powdered X-ray method, it is important that the extent of transformation (if available from the run data) be recorded for each data point. An example of Skippen's summary of run data for a mixed-volatile reaction is shown in Figure 5a. It is important to note the error band for the equilibrium boundary (Fig. 5a); Skippen chose an equilibrium curve that approximately passes through the midpoint of the error bracket, and his equilibrium constants were derived without regard to the error band. This error has been considered, however, in a more recent treatment of his data (Skippen, 1974). A drawback with Skippen's technique stems from the fact that he did not determine the gas composition at the end of a run. His calculated gas compositions are subject to several sources of error including: (a) uncertainty in the tabulated equilibrium constants, (b) incomplete equilibration of the gas in the inner capsule with the buffer, (c) non-ideal mixing in the fluid, and (d) errors in the fugacity coefficients from reduced variable charts. The combined error of all of the above factors is very difficult to evaluate.

In view of the diverse experimental approaches to mixed-volatile equilibria, interlaboratory comparison is very useful. If we consider *only* studies where reaction reversibility has been carefully documented, the system CaO-MgO-SiO_2-H_2O-CO_2 provides the best opportunity for interlaboratory comparison. Slaughter, Kerrick, and Wall (1974) have shown that for this system there is good agreement between the experimental equilibrium brackets obtained by various laboratories.

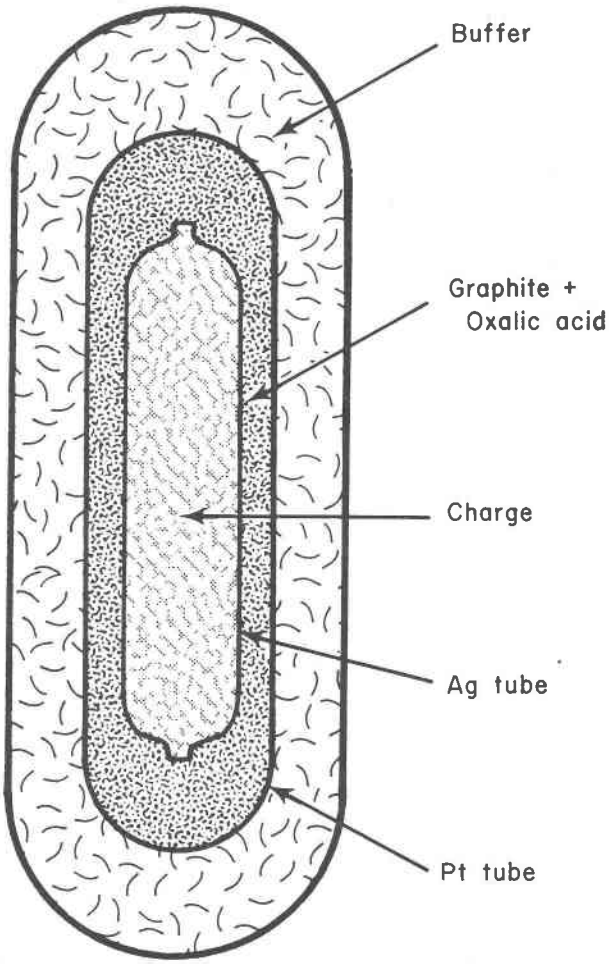

FIG. 11. Capsule arrangement for buffered experiments with a C-O-H gas in equilibrium with graphite (from Eugster and Skippen, 1967).

T-X Equilibria for Chemical Systems

This section is an analysis of chemical systems relevant to metamorphic assemblages. It is important to note that only equilibria which have been experimentally determined, or which can be derived from accurately located invariant points, are considered in this analysis. Furthermore, this analysis considers

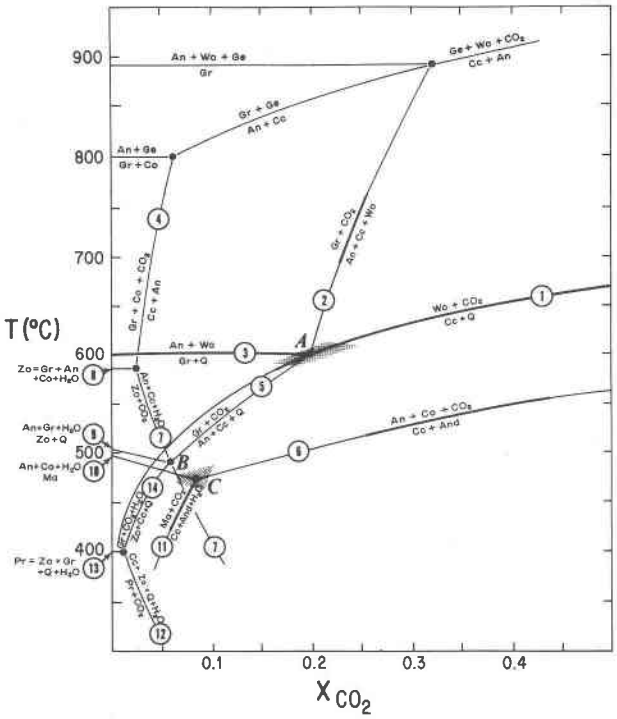

FIG. 12. T-X_{CO_2} diagram at $P_f = 2$ kbar for some equilibria in the system CaO-Al_2O_3-SiO_2-CO_2-H_2O. Sources for equilibria in pure H_2O ($X_{CO_2} = 0$) are: reactions (3), (8), and (9), Boettcher (1970) and Newton (1966); reaction (13), Liou (1971); reaction (10), Velde (1971). Heavy lines represent experimentally determined portions of equilibria whose sources are: reaction (1), Greenwood (1967b); reaction (2), Gordon and Greenwood (1971); reactions (6) and (11), Nitsch and Storre (1972). Shaded areas are the estimated errors in location of invariant points resultant from errors in the experimentally determined equilibria intersecting to form invariant points.

only stable equilibria—Skippen (1974) and Finger and Burt (1972) present detailed examples illustrating the selection of stable equilibria within a chemical system.

Space does not permit presentation of T-X sections for each chemical system at a wide variety of pressures. In general, the pressures chosen for these diagrams are those at which most experimental data exist.

Except for Figure 13, equilibria were extrapolated either graphically or by computer calculations.

The System: CaO-Al_2O_3-SiO_2-CO_2-H_2O

This system provides a reasonable approximation to the bulk composition of many impure limestones, in that it includes common calc-silicate minerals such as wollastonite, grossularite, anorthite, and zoisite, as well as somewhat rarer phases such as margarite and gehlenite.

A T-X section at $P_f = 2$ kbar (Fig. 12) shows the location of invariant point A, which appears to be well established since it involves intersection of three experimentally determined reactions. T-X loci of equilibria involving zoisite and margarite are less certain. There has been particular disagreement about the location and slope of reaction (7) in Figure 12. Some workers (Storre, 1970; A. B. Thompson, 1971) have considered this equilibrium to have a positive slope, whereas others derived a negative slope (Kerrick, 1970; Gordon and Greenwood, 1971). Experimental data of Storre and Nitsch (1972), moreover, suggests that the equilibrium curve is essentially vertical in the 450–550°C range. However, their experimental data are difficult to interpret since they obtained anomalous results in runs with pure CO_2 as the pressure medium (*i.e.*, the open squares on the 2 kbar data of Figure 2 of Storre and Nitsch, 1972). In Figure 12 invariant point B was located by the intersection of reaction (9), as extrapolated from the experimentally determined point in pure H_2O, with reaction (5), extrapolated from invariant point A. Considering errors, invariant point B could be as H_2O-rich as $X_{CO_2} \simeq 0.03$ at $T \simeq 450$°C. In this case there would be relatively little incompatibility with the equilibrium boundary for reaction (7) given by Storre and Nitsch (1972). We conclude that $P_f = 2$ kbar, and in the moderate temperature range of metamorphism, grossularite, zoisite, and margarite are indicative of a H_2O-rich fluid. With increasing pressure to 7 kbar there appears to be no major topologic changes (see Fig. 15).

The only margarite equilibria shown in Figure 12 are those outlining the maximum stability of this phase. Frey and Orville (1974) show additional reactions involving margarite in this system, as well as a topology for equilibria where Na_2O is an additional component.

Topologic relations in the low temperature range ($T < 400$°C) are not shown in Figure 12, primarily because there are considerable discrepancies concerning the location of stable equilibria. Furthermore, H_2O-CO_2 mixtures depart markedly from ideality in this temperature range; thus, calculations based on ideal mixing may be in considerable error.[11] We can, however, outline the most general aspects of low-temperature T-X equilibria, based on recent analysis by Wall and Essene (1972), Nitsch and Storre (1972),

[11] Ryzhenko and Malinin (1971) do not present fugacity coefficients for H_2O–CO_2 mixtures below 400°C.

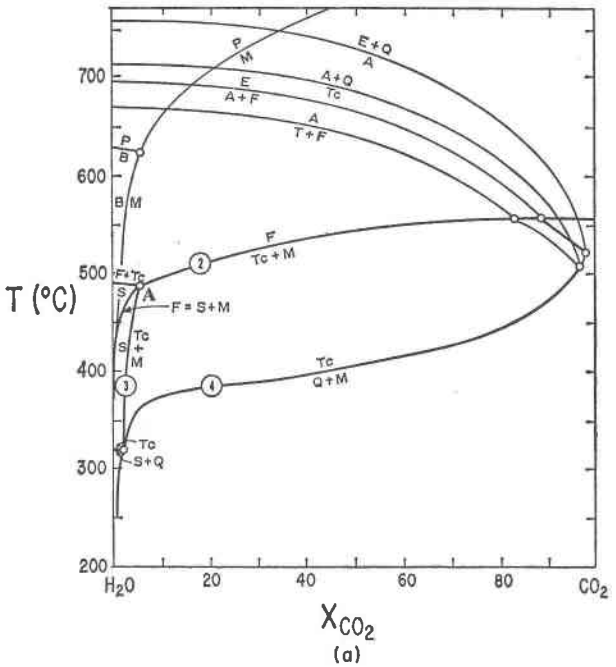

FIG. 13. (a) Equilibria in the system MgO-SiO_2-CO_2-H_2O at $P_f = 2$ kbar (from Johannes, 1969); the heavy lines represent experimentally investigated equilibria. Topology of equilibria near the right margin of the diagram is shown in Figure 13b.

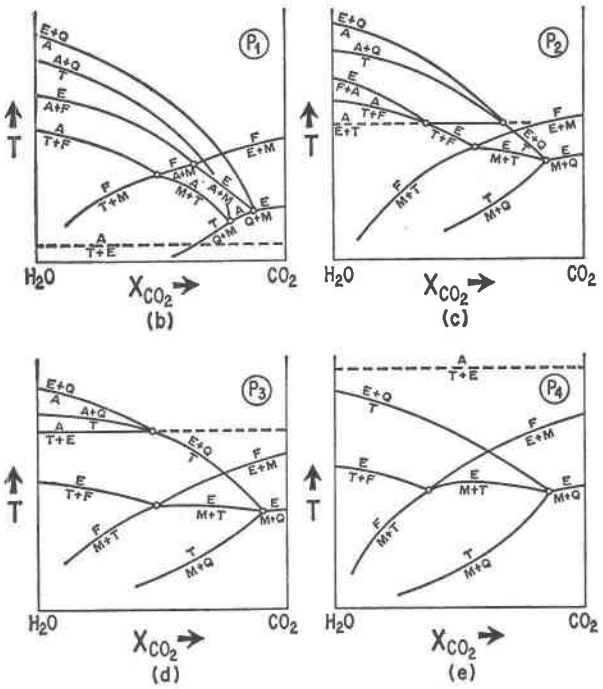

FIG. 13. (b) Schematic diagram clarifying the topology shown near the right margin of Figure 13a. (c, d, e) Topologic changes of equilibria shown in Figure 13b in going toward higher pressure ($P_1 < P_2 < P_3 < P_4$; from Evans and Trommsdorff, 1974).

and Nitsch (1972). At low temperatures, zoisite will be confined to relatively H_2O-rich fluids by reactions such as:

margarite + calcite + quartz

$$= \text{zoisite} + CO_2 + H_2O,$$

margarite + calcite + pyrophyllite

$$= \text{zoisite} + CO_2 + H_2O$$

Wairakite and laumontite, stable in the moderate to low pressure range ($P_f < 4$ kbar), as well as the chemically equivalent high-pressure assemblage, lawsonite + quartz, are restricted to H_2O-rich fluids. Xonotolite, the hydrated, low temperature equivalent of wollastonite (Buckner, Roy, and Roy, 1960), will be confined to H_2O-rich fluids by the reaction:

$$\text{xonotolite} + CO_2 = \text{calcite} + \text{quartz} + H_2O$$

Schematic T-X topologies at low temperature and at high pressure, showing additional equilibria involving zoisite and lawsonite, are presented by Chatterjee (1971).

The System: MgO-SiO_2-CO_2-H_2O

This system provides an excellent approximation to the bulk composition of metamorphosed ultrabasic rocks.

Johannes (1969), who provides the most recent summary of experimental data in this system, obtained a reversal on only one equilibrium (reaction (3) in Figure 13a). His equilibrium boundary for reaction (2) is supported by the reversal determined by Greenwood (1967a); furthermore, Johannes' (1969) data on serpentine stability agree with the experimental data of other workers on serpentine stability in pure H_2O.[12] However, there is marked disagreement between the experimental data of Johannes for reaction (4), and that calculated by Greenwood (1967a). Considering the fact that Johannes' experiments approached the equilibrium boundary from the high temperature side only, it is possible that his curve represents an *upper* stability limit for this reaction, rather than the actual *T-X* location of the

[12] It should be noted, however, that considering scatter in his data for reaction (3) at 2 kbar (see Johannes, 1969, Fig. 2), considerable error is possible in location of invariant point A, and, hence, in location of the upper temperature stability limit of serpentine.

equilibrium boundary. If so, his apparent attainment of equilibrium on reaction (2), which was approached from the high temperature side only, may reflect the positive effect of temperature on reaction kinetics (reaction (2) lies at higher temperature than reaction (4)). Figure 13 (b)–(d) illustrates the profound effect of pressure change on the *T-X* topology of this system. As shown in Figure 13, this system contains numerous minerals and mineral assemblages, such as brucite and anthophyllite + magnesite, which provide excellent indicators of intensive variables during metamorphism.

The System: CaO-MgO-SiO_2-H_2O-CO_2

This system provides an approximation to the bulk composition of siliceous dolomites. A recent compilation of equilibria and comparison with previous investigations is given by Slaughter, Kerrick, and Wall (1974). Thus, the reader is referred to their paper for a detailed discussion. In this system there is reasonable agreement between the experimental data of Skippen (1971), Gordon and Greenwood (1971), and Slaughter, Kerrick, and Wall (1974). Experimental determination by Metz (1970) of reaction (6) (Fig. 14) suggests considerably higher equilibrium temperatures than those obtained by other investigators. Since Metz did not elaborate on the histories of capsules reported to be on the low-temperature side of the equilibrium (as discussed previously), it is *possible* that Metz inadequately demonstrated reversibility; if so, his data provide a maximum temperature for this reaction. This conclusion is strengthened by the fact that Slaughter, Kerrick, and Wall (1974), using several independent techniques to investigate this reaction, suggest equilibrium at lower temperatures than implied by Metz. Location of invariant point **A** in Figure 14 appears to be quite accurate. However, because of the low-angle intersection of equilibria, invariant point **B** is subject to a large error (most of which is error in X_{CO_2}). As pointed out by Slaughter, Kerrick, and Wall (1974) the *T-X* location of equilibria involving forsterite (dashed lines in Figure 14) are subject to extreme uncertainty. Major important conclusions regarding particularly instructive assemblages are: (a) talc + calcite is confined to a relatively small area of *T-X* space, (b) dolomite + diopside *may* indicate rather CO_2-rich fluids, and (c) at moderate temperatures (400–500°C) dolomite + quartz is stable only in a relatively CO_2-rich fluid.

T-X sections for this system at various pressures are shown by Skippen (1974) and by Slaughter, Kerrick, and Wall (1974). A point of disagreement between these studies concerns the pressure effect

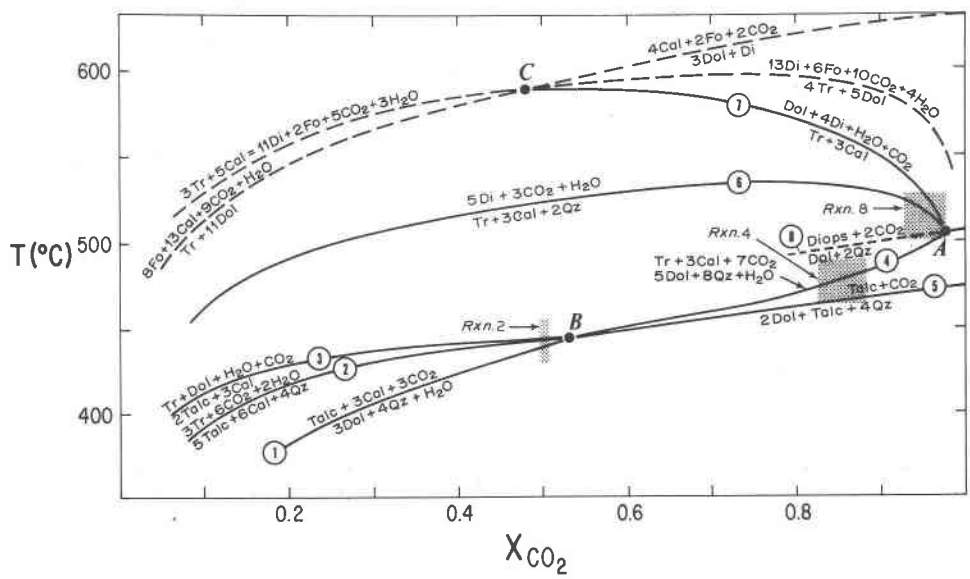

FIG. 14. Some equilibria in the system CaO-MgO-SiO_2-CO_2-H_2O at $P_f = 2$ kbar (from Slaughter, Kerrick, and Wall, 1974). Solid lines represent equilibria whose locations are reasonably accurate, whereas dashed lines are reactions whose locations are extremely uncertain. Shaded areas are experimental equilibrium brackets obtained by Slaughter, Kerrick, and Wall (1974).

on the stability field of the assemblage talc + calcite, bounded by reactions (1) and (3). The reader is referred to the above papers for discussion of this topic.

The System: K_2O-CaO-MgO-Al_2O_3-SiO_2-CO_2-H_2O

Comparatively little experimental work has been carried out on equilibria involving potassic phases in this system, which provides a model for reactions involving phlogopite, muscovite, and K-feldspar, the common constituents of metamorphosed impure limestones and calcareous pelites. Strictly speaking, we should include in this system all equilibria in the subsystems discussed previously. However, to avoid repetition, we will confine most of our attention to equilibria not shown on Figures 12–14. Most reversals have been obtained only at high pressures (6–7 kbar), as summarized in Figure 15. The data of Johannes and Orville (1972) should be regarded as tentative since there was no elaboration on their experimental techniques or run data. Run data for reaction (7), as plotted on their *T-X* diagram, appears ambiguous. Invariant point **D** was located by extrapolation of reaction (4) from invariant point **A**. However, independent calculations on the *T-X* locus of reaction (1) at 7 kbar suggest that invariant point **D** should be at $X_{CO_2} \leq 0.15$. Such modification of invariant point **D** would necessitate shifting invariant point **A** to the left. Hence, reaction (7) *may* lie at more H_2O-rich compositions than shown in Figure 15. Preliminary experimental data obtained in our laboratory suggests that invariant point **C** may shift toward lower X_{CO_2} with decreasing pressure (at $P_f = 2$ kbar, the invariant point is tentatively located at $T \simeq 450°C$, $X_{CO_2} < 0.10$). The pressure effect on the *T-X* location of some equilibria involving potassic phases is outlined by Hewitt (1973a) and by Hoschek (1973).

Hewitt (1973a) presents a *T-X* topology at $P = 6$ kbar showing additional equilibria in this system. In addition, a *schematic* *T-X* topology showing numerous additional equilibria within this system (involving phases such as lawsonite, chlorite, and chloritoid) is illustrated by Chatterjee (1971).

Invariant point **E** was obtained by the intersection of reactions (8) and (16), which were extrapolated from lower pressure equilibrium brackets by assuming ideal mixing in the fluid. Reaction (17), which passes through this invariant point, limits the assemblage dolomite + K-feldspar to CO_2-rich fluids at elevated temperature (see also Carmichael, 1970, p. 177–180).

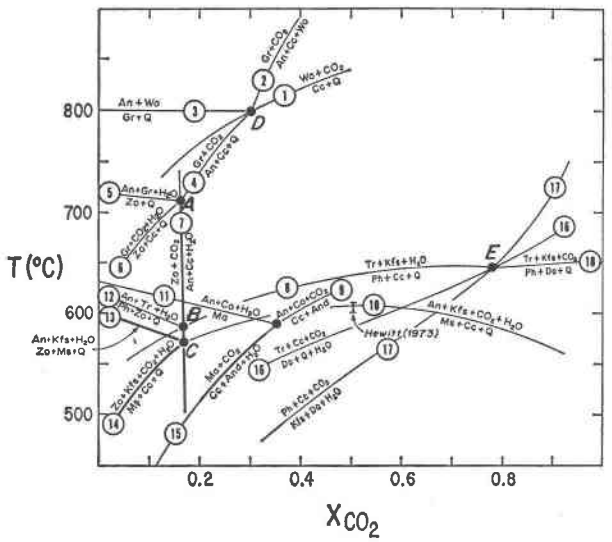

FIG. 15. T-X_{CO_2} diagram at $P_f = 7$ kbar for some equilibria in the system K_2O-CaO-MgO-Al_2O_3-SiO_2-CO_2-H_2O. Sources for equilibria in pure H_2O are: reactions (3) and (5): Boettcher (1970) and Newton (1966); reaction (11), Velde (1971). Heavy lines represent experimentally determined equilibria, whose sources are: reactions (7), (13), and (14), Johannes and Orville (1972); reaction (15), Nitsch and Storre (1972). Reaction (8) was extrapolated from Hoschek's (1973) data at 6 kbar, and reaction (16) was extrapolated from the data of Slaughter, Kerrick, and Wall (1974).

Other Systems

Certain mixed-volatile equilibria have been experimentally determined for other chemical systems, such as reactions involving sphene (Kerrick, Hunt, and Wall, 1973), humite-group minerals (Becker and Hoschek, 1973; Tell, 1974), and Mn-bearing phases (Peters, Schwander, and Trommsdorff, 1973). *T-X* equilibria in systems other than outlined above are schematically shown by Kerrick, Crawford and Randazzo (1973), for reactions involving idocrase and scapolite, by Burt (1972b) for the system FeO-Fe_2O_3-SiO_2-H_2O-CO_2 (involving mixed-volatile equilibria occurring in metamorphosed iron formations), and by Frey and Orville (1974) for equilibria involving sodic phases (*i.e.*, albite and paragonite). From thermochemical data, Glassley (1974) calculated the *T-X* loci of low-grade equilibria in the system CaO-MgO-Al_2O_3-SiO_2-CO_2-H_2O.

Field Relations

Introduction

Interpretation of mixed-volatile equilibria in natural systems is complicated by the combined effects of

several variables, including some that are extremely difficult to evaluate, such as kinetic factors, varying P-T conditions, and disequilibrium. Indeed, it is difficult to find geological examples where it is possible to study the effect of only one variable (*e.g.*, H_2O-CO_2 mixtures) without possible complications by a host of other factors. However, with a firm grounding in the theory of mixed-volatile equilibria and with an understanding of complicating factors, considerable progress can be made in elucidating the role of mixed-volatiles in natural parageneses. Hopefully this will lead to the selection and thorough study of geological examples whereby mixed-volatile equilibria can be investigated with a minimum of complicating factors. In summarizing the results of field investigations on this topic, it is necessary to first point out potential complications in interpretation of the role of mixed-volatiles in natural parageneses.

Vapor-Present vs Vapor-Absent Metamorphism

T-X diagrams assume the presence of a fluid[13] phase. However, it is entirely possible that rocks could undergo metamorphism by escape of H_2O and CO_2 along grain boundaries, either in a very thin intergranular film, or by movement along dislocations in solids adjacent to grain boundaries. Because of the lack of a discrete vapor phase, such a system is referred to as "vapor absent." Elliott (1973) suggests that grain boundaries in rocks undergoing metamorphism are only one or two atomic layers thick. If so, it is probable that the physical and thermodynamic properties of such a fluid would be affected by charge imbalances and dislocations at adjacent grain boundaries. Greenwood (1961) provides an excellent summary of this subject, as well as implications as to the thermodynamic properties of the fluid. Thus, we shall only mention here the fact that in vapor-absent metamorphism, the chemical potentials of both H_2O and CO_2 will be lower than if these components were present in a vapor phase (Greenwood, 1961, p. 3944). As shown on a $\mu_{H_2O} - \mu_{CO_2}$ diagram, lowering the chemical potential of one or both of these species at fixed P_s and T could lead to the production of "higher grade" assemblages than would be present with vapor saturation. The assumption of vapor-saturated conditions, however, is strengthened by the fact that many metamorphic minerals have fluid inclusions. That some inclusions are primary is supported by recent investigations which show that the composition of the fluid within inclusions is compatible with that obtained by independent evidence of T-X equilibria as applied to solid assemblages (Trommsdorff, 1972, p. 570; Evans and Trommsdorff, 1974). Evidence for vapor-saturated conditions in low-grade rocks stems from abundant veins, from occasional cavities containing metamorphic minerals (Ernst, 1972; Essene and Fyfe, 1967), and from fluids permeating rocks undergoing contemporary low-grade metamorphism (Muffler and White, 1969).

P_{fluid} *vs* P_{solids}

In applying T-X equilibria to natural systems it is assumed that $P_f = P_s$ during metamorphism. However, if a rock has strength, it is possible to maintain a condition whereby $P_f \gtrless P_s$. Implications of this condition have been discussed by several investigators (*e.g.*, Winkler, 1967, p. 10–11), although special emphasis has been given to the effect of $P_f < P_s$ (*e.g.*, J. B. Thompson, 1955; Althaus, 1968). On a T-X projection at fixed P_s, progressive lowering of P_f produces much the same effect on mixed-volatile reactions as was outlined previously for progressive addition of volatiles other than H_2O and CO_2 to the fluid. The condition $P_f < P_s$ is one of mechanical instability and thermodynamic disequilibrium; it results in a driving force for recrystallization to reduce the total volume of pore fluid, and thus increase P_f (Greenwood, 1961, p. 3943). Rock strength is an inverse function of P_s, P_f, and T; thus, inequality of P_f and P_s should be most marked in regimes of low-pressure, low-temperature metamorphism, such as the zeolite facies. Coombs *et al* (1959) and Nakajima and Tanaka (1967) discussed examples of zeolite facies assemblages whereby the mineral parageneses may reflect variations in the P_f/P_s ratio during metamorphism; thus laumontite or analcite formed in relatively porous rocks, whereas the "low-grade" equivalent (heulandite or mordenite) formed in intimately associated stratigraphic units with lower porosity. As observed in thin section, most low-grade metamorphic equivalents of rocks that had considerable porosity, such as graywackes and sandstones, now consist of a close-knit aggregate of grains with no evidence of porosity. This suggests

[13] As used here the term "fluid" carries no connotation as to the exact physical properties of this phase. Under conditions of low pressure and high temperature this phase is more akin to a gas than to a fluid; in addition, the gaseous nature becomes more marked with increasing CO_2/H_2O ratio.

that recrystallization has been moderately efficient in reducing the porosity. It is well known that marbles readily recrystallize (Heard, 1963). Furthermore, it is probable that quartz-rich rocks recrystallize rapidly, particularly in the presence of some H_2O (Hobbs, 1968). Elevated P_f would also be maintained by relatively large amounts of volatiles that would be released during prograde metamorphism. It would appear, therefore, that it is reasonable to assume that most rocks underwent metamorphism with $P_f \simeq P_s$.

Solid Solution and Mixed-Volatile Equilibria

To date, most experimental data on mixed-volatile equilibria has been obtained for "pure" systems containing end-members of solid solution series. Obviously, the role of solid solution must be taken into account in order to apply *T-X* equilibria adequately to natural systems. On a *T-X* diagram, changes in composition of solid solution phases will cause shifts in the loci of equilibria involving these phases. Calculation of the loci of *T-X* curves for specific solid solution compositions is readily made through the equilibrium constant, as outlined in numerous studies (Eugster and Skippen, 1967; Ghent and DeVries, 1972; Kerrick, Crawford, and Randazzo, 1973; Hewitt, 1973a). Unfortunately, the scarcity of thermodynamic data for many solid solution minerals frequently necessitates that such calculations be made with the assumption of ideal mixing in the solids.

An example of the effect of solid solution on *T-X* equilibria is illustrated in Figure 16. Two adjacent rock domains metamorphosed at the same P_f, T, and X_{CO_2} could have contrasting assemblages resulting from differences in solid solution composition only. Thus, for example, at point **X** in Figure 16 a Na-poor system would contain grossularite, whereas a Na-rich rock (dashed lines) would have plagioclase + wollastonite + calcite. In this case, neglecting the effect of solid solution in plagioclase would lead to the erroneous conclusion that the vapor phase in the sample containing grossularite was more H_2O-rich than that with the assemblage plagioclase + wollastonite + calcite.

It will undoubtedly be some time until activity data for rock-forming solid solutions is obtained over a wide range of temperature. Some progress has been made on obtaining activity data for several phases of interest in mixed-volatile equilibria, namely, plagioclase (Orville, 1972), epidote-group minerals (Holdaway, 1972), grossularite (Holdaway, 1972),

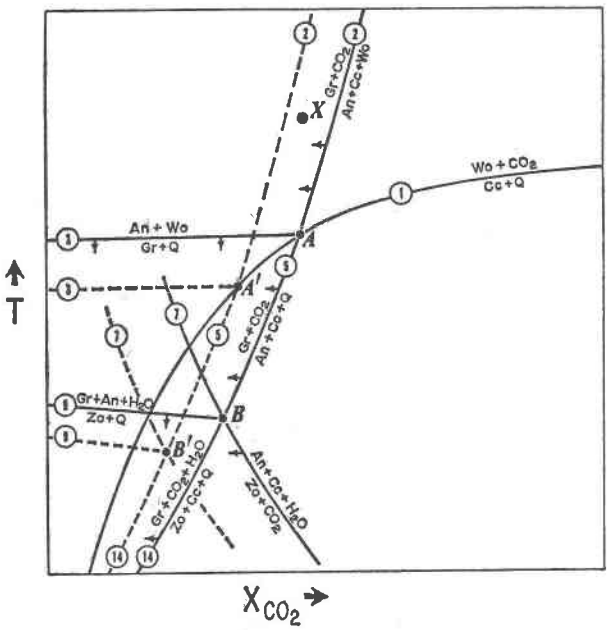

FIG. 16. Schematic diagram for equilibria in the system CaO-Al_2O_3-SiO_2-CO_2-H_2O (solid lines). Arrows show shift of equilibria resulting from progressive addition of albite to plagioclase. Dashed lines represent equilibria for a fixed composition of plagioclase. Point **X** is discussed in the text. Calculation of curves for fixed plagioclase composition is outlined by Kerrick, Crawford, and Randazzo (1973).

orthopyroxene (Navrotsky, 1971), and olivine (Saxena, 1972).

The role of solid solution in mixed-volatile equilibria has been considered by several investigators (Kerrick, 1970; Kerrick, Crawford, and Randazzo, 1973; Ghent and DeVries, 1972; Crawford, 1972; Hewitt, 1973a; Frey and Orville, 1974). In some cases solid solution has exercised an important role in maintaining activity gradients in the pore fluid between nearby domains (Kerrick, Crawford, and Randazzo, 1973); in contrast, there are other cases where the composition of solid solution phases was apparently controlled *by* a gradient in fluid composition (Hewitt, 1973a).

Variations in the composition of solid solutions can have a profound effect on *T-X* topologies. Starting with equilibria involving end-members of solid solution series, the *T-X* loci of reactions can be adjusted for solid solution using an integrated form of the expression:

$$\Delta Sr\ dT = RT\ d \ln K$$

Topologies with solid-solid reactions will be most affected by solid solution, as these reactions have

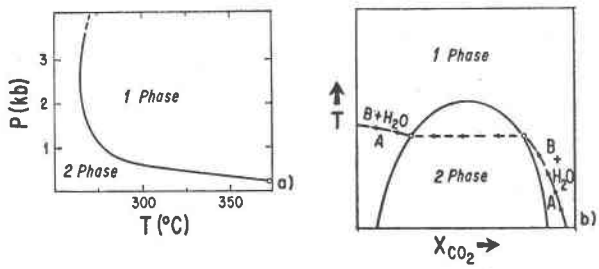

FIG. 17. (a) *P-T* locus of critical curve (crest of solvus) for $H_2O + CO_2$ (from Tödheide and Franck, 1963). (b) Schematic T-X_{CO_2} diagram showing H_2O-CO_2 solvus, and prograde path for buffered dehydration reaction crossing the solvus.

comparatively small entropy changes. This effect is well illustrated by Evans and Trommsdorff (1974) for the system MgO-SiO_2-CO_2-H_2O, who show that relatively small amounts of iron in solid solution could profoundly alter the *P-T* location of the solid-solid reaction:

$$\text{enstatite} + \text{talc} = \text{anthophyllite},$$

resulting in a profound effect on the topology shown in Figure 13.

Non-Binary Fluids in Metamorphism

As previously outlined, compositional departures from binary H_2O-CO_2 fluids will be most important in graphite-bearing systems at low f_{O_2}. As shown in Figure 7, profound differences in composition of a C-O-H fluid could be produced by varying f_{O_2}; thus, assemblage contrasts related by mixed-volatile equilibria could reflect corresponding variation in f_{O_2}. Clearly, a thorough search for an assemblage that defines f_{O_2}, such as biotite + K-feldspar + magnetite (Wones and Eugster, 1965) or magnetite + ilmenite (Buddington and Lindsley, 1964), could aid considerably in quantifying fluid compositions in graphite-bearing assemblages.

Numerous workers have calculated fluid compositions in graphite-bearing systems with the assumption that the atomic H/O ratio is fixed at 2/1 (French, 1966, p. 241; Morgan, 1970). This ratio is equivalent to that of H_2O, and, hence, it is referred to by some as a fluid of "pure water" composition (Morgan, 1970). For a fluid with H/O = 2, graphite becomes a true oxygen buffer (in the three component C-O-H system, this additional compositional restriction yields a variance of two, and it is only necessary to fix P and T in order to calculate the fluid composition). This compositional restriction would appear to approximately hold only in rocks undergoing dehydration reactions, where the fluid composition would largely be controlled by the release of H_2O from breakdown of hydrous minerals. However, with carbonate-bearing assemblages, concomitant decarbonation reactions would profoundly alter the pore fluid composition from that of H/O = 2 (release of CO_2 would lower the H/O ratio).

In some graphite-bearing carbonate assemblages, an additional restriction which aids in determining the composition of the fluid stems from equation (5), as listed on the section on non-binary fluids in the C-O-H system. Ghent, Jones, and Nicholls (1970) calculated P_f as a function of f_{O_2} for a graphite-bearing greenschist facies assemblage. Their calculations show that P_f is very sensitive to f_{O_2}, such that reasonable pressures ($P_f \simeq 6$ kbar) are obtained only within a relatively narrow range of f_{O_2}; unreasonably high fluid pressures (> 10 kbar) are obtained with f_{O_2} just outside of this range. Thus, limitation to reasonable values of P_f can considerably aid in quantifying the composition of fluids in some graphite-bearing systems.

Graphite is very common in metamorphosed pelitic assemblages (Miyashiro, 1964); consequently, interpretation of pelitic systems with a model of $P_{H_2O} \simeq P_f$ may be considerably in error. Calculations by Guidotti (1970) and Jones (1972) suggest that the deviation of P_{H_2O} from P_f is significant in graphite-bearing metapelitic assemblages of Barrovian-type regional metamorphism. Based on experimental data on muscovite + quartz decomposition in H_2O-CO_2 mixtures, coupled with stability relations of the Al_2SiO_5 polymorphs and with the minimum melting of granite, Kerrick (1972) concluded that upper amphibolite facies metamorphism of graphite-bearing pelites occurred with pore fluids having compositions (X_{H_2O}) from 0.5 to 0.9.

Non-Ideal Mixing and Unmixing of Fluids in Low-Grade Rocks

Considering all *P-T* regimes of metamorphism, mixed-volatile equilibria in low-grade rocks should show rather unique behavior because of unmixing and strong departure from ideal mixing in the fluid phase. Large positive deviations from ideality, as suggested by extrapolation of Greenwood's (1973) data, are compatible with unmixing of H_2O and CO_2. Buffered prograde mixed-volatile reactions crossing the H_2O-CO_2 solvus, such as that illustrated in Figure 17b, would undergo a marked change in

fluid composition. On a *P-T projection* there would be a break in slope of this equilibrium, primarily reflecting a discontinuity in the entropy of mixing for the volatiles in the particular equilibrium considered. It may be possible to trace such a change in fluid chemistry by a thorough study of fluid inclusions in a rock sequence subjected to low-grade metamorphism. It should be noted that H_2O-rich fluids apparently stabilized many common assemblages in low-grade rocks (Nitsch, 1972; Ernst, 1972; A. B. Thompson, 1971; Liou, 1971b; Glassley, 1974); thus, many low-grade sequences may have been metamorphosed on the H_2O-rich side of the solvus. Assemblages indicative of more CO_2-rich fluids, such as those showing direct transitions from indurated sediments to greenschist facies assemblages (Zen, 1961; Albee and Zen, 1969; Liou, 1970; Coombs, Norodyski, and Naylor, 1970), are those most likely to have been metamorphosed in the presence of a two-phase fluid. Although blueschist facies metamorphism was accompanied by H_2O-rich fluids (Ernst, 1972), some variation in the a_{H_2O} is necessary to explain contrasting assemblages (Kerrick and Cotton, 1971; Ernst, 1972).

Local vs External Control of Fluid Composition in Metamorphism

The subject of local *vs* external control of fluid composition has been the subject of considerable debate (*e.g.*, Weill and Fyfe, 1967; Korzhinskii, 1967; J. B. Thompson, 1970). Moreover, even the relevant terminology varies. Thus, locally controlled components have been referred to as "inert" components (Korzhinskii, 1959), "initial value" components (Zen, 1963), and "J" components (J. B. Thompson, 1970), whereas components with externally controlled chemical potentials have been referred to as "perfectly mobile" components (Korzhinskii, 1959), "boundary value" components (Zen, 1963), and "K" components (J. B. Thompson, 1970). For "mobile" *vs* "inert" behavior, the system can be referred to as being "open" or "closed," respectively, to the component under consideration. As used here, these terms refer *only* to the local *vs* external control of the chemical potentials, and do not necessarily carry implications as to the physical mobility of the components under consideration. The basic difference between local *vs* external control of chemical potentials of fluid components is illustrated in Figure 18. Consider the prograde, isobaric *T-X* path of an initial assemblage; calcite + quartz, with a fluid composition X_1. Prograde metamorphism increases temperature to point 2, at which the first trace of wollastonite appears. With open system behavior, calcite and/or quartz will decompose to wollastonite at point 2, such that, depending upon the initial proportion of calcite *vs* quartz, either wollastonite, wollastonite + calcite, or wollastonite + quartz will remain at higher temperatures. Thus, with the system open to H_2O and CO_2, the assemblage, wollastonite + calcite + quartz, is stable only at an invariant point. In a closed system, wollastonite will join the assemblage calcite + quartz upon reaching point 2, and the system will follow along the equilibrium boundary with the reaction "buffering" the composition of the pore fluid until calcite, quartz, or both, are consumed.[14] Buffering requires the reaction rate to be fast, such that temperature changes are immediately accompanied by fluid compositional changes resulting from evolution of CO_2 by the reaction. Clearly, intermediate paths between the two extremes, such as c in Figure 18, are possible where reaction rate is not fast enough to strictly buffer the fluid composition, yet the reaction produces an increase in X_{CO_2} with progressive increase in temperature. Path c would imply chemical dis-

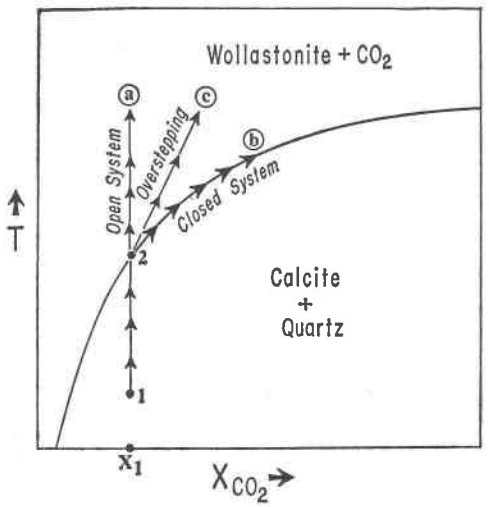

FIG. 18. Illustration of open *vs* closed behavior with regard to volatile components in a representative mixed-volatile reaction.

[14] Because formation of a product requires a finite overstepping, the path of buffering is likely to occur as a series of small steps along the equilibrium boundary, each with a vertical segment corresponding to overstepping, followed by an isothermal change in the fluid composition to the equilibrium curve.

equilibrium, since the assemblage calcite + quartz would occur outside of its stability field. This behavior would be possible with relatively poor permeability of the system with regard to fluids.[15] It is important to point out that textural disequilibrium in thin section, such as the replacement of calcite + quartz by wollastonite, does not necessarily imply chemical disequilibrium. Such a texture could be fully compatible with an arrested prograde buffer reaction.

Gordon and Greenwood (1971, p. 1685–1687) provide a concise summary of field investigations concerning the open *vs* closed behavior of metamorphic systems. They conclude that both open and closed behavior have been described in regional and contact metamorphism, such that: "Each natural occurrence must be carefully judged on the basis of its own characteristics and a decision reached, if possible, as to whether the system was perfectly open, completely closed, or buffered by local domains such as original sedimentary layers." One point should be raised, however, concerning the paper by Carmichael (1970), which is included in Gordon and Greenwood's (1971) summary. Carmichael (1970, p. 181) notes a reentrant in the Ca-amphibole-K-feldspar isograd where it crosses a graphite-bearing calcareous unit. While his description of the isograd implies a strong tendency toward open system behavior, the calcareous unit described above would, in contrast, suggest some local control of fluid composition. Since publication of Gordon and Greenwood's paper, Crawford (1972) and Kerrick, Crawford, and Randazzo (1973) have described contact metamorphosed calcareous rocks which appear to have had very local control of fluid composition. Chatterjee (1971, p. 225–226) suggests very steep gradients (*i.e.*, local control) of the H_2O/CO_2 ratio during low-grade metamorphism of rocks in the western Italian Alps. In the Damara Belt of South West Africa, Puhan and Hoffer (1973) described assemblages in siliceous dolomites indicative of internal control (buffered reactions) during prograde metamorphism. Trommsdorff (1972) has suggested that regionally metamorphosed siliceous dolomites in the Alps were closed with respect to CO_2 and H_2O. As shown by Trommsdorff (1972) the *T-X* paths, during prograde metamorphism, of assemblages buffering the fluid can be quite complex, such that for certain assemblages the fluid composition can alternatively move toward CO_2-rich and CO_2-poor compositions upon increasing temperature. Greenwood (1967a) provides an excellent summary of the complexity of prograde buffering in the developement of contrasting assemblages. The example described by Trommsdorff (1972) shows an orderly progression of buffered reactions compatible with a self-consistent *T-X* topology—this gives strength to the argument that the assemblages represent true buffering and not disequilibrium as described by path c in Figure 18. Buffering provides an effective mechanism by which, for example, an assemblage with a H_2O-rich fluid at low grade could end up with a CO_2-rich fluid at higher grade. Trommsdorff's paper also illustrates the usefulness of field relations as an independent means of deducing *T-X* topologies, although there remains some controversy regarding the high pressure topology in the CaO-MgO-SiO_2-CO_2-H_2O system (Slaughter, Kerrick, and Wall, 1974). An important point to be emphasized here is the need for a detailed integration of field and experimental data in understanding the role of mixed-volatiles in metamorphism.

Recently, cases have been described where the system appears to have changed from closed to open behavior with time. Cermignani and Anderson (1973) describe an amphibolite facies assemblage where they conclude that diopside layers initially formed from a siliceous dolomite in a closed system; subsequent late-stage introduction of H_2O (open system) formed tremolite + calcite at the borders between the diopside layers and the host dolomite. In regionally metamorphosed ultramafics in the Lepontine Alps, Evans and Trommsdorff (1974) suggest early prograde buffering of the fluid phase (closed system behavior), followed by late-stage veining by CO_2-rich fluids whose chemical potentials were externally controlled. In this example, the change from closed to open behavior is quite obvious from the "plumbing system." Thus, closed system behavior is more likely in a compact rock undergoing slow devolatilization, where the proportion of fluid at any one time is very small. In contrast, the late-stage veining introduced large amounts of CO_2 such that, because of the relatively large mass of fluid in relation to the solids, local buffering was ineffective in controlling the fluid composition. Hewitt (1973b) described a Barrovian metamorphic sequence of interbedded pelitic schists and impure marbles where assemblage zoning at the edges of the marble appears to reflect steep gradients

[15] With $P_f = P_s$, prograde buffering of the reaction shown in Figure 18 requires expulsion of some pore fluid in a system with constant porosity.

in the fluid composition.[16] Hewitt maintains that prograde metamorphism of the marbles was accompanied by internal buffering until one of the reactants disappeared. Then open system behavior resulted from the influx of water from dehydration in the surrounding schist, causing a decrease in X_{CO_2} until another reaction is intersected whereupon further buffering occurred with increasing temperature.

Mixing of fluids between adjacent rock domains is a function of permeability, and amounts of volatiles given off by each lithology as a function of time. Hewitt (1973b) has considered these factors in some detail. If, for example, a marble gives off more fluid than a surrounding pelite, mixing of fluids will occur on the pelite side of the contact; the reverse is true if the pelite gives off more fluid than the marble. The mixing could change as a function of time; thus, decarbonation reactions could occur in the marble at a time when no dehydration reactions are occurring in the pelite; this could imply closed system behavior in the marble and open system behavior in the pelite because of influx of CO_2 from the adjacent marble. Later in the metamorphism, dehydration reactions could occur in the pelite, while no reactions occurred in the marble, to produce an influx of H_2O from the surrounding pelite.

It is useful to obtain an idea of the "buffer capacity" of a rock using a simple example. Let us assume that we have a calcite marble with 10 wt percent quartz, a small amount of pore fluid ($X_{CO_2} = 0.5$), and a negligible amount of wollastonite. In this example, consider influx of H_2O from dehydration reactions in a surrounding pelite, and that the reaction:

$$\text{calcite} + \text{quartz} \rightarrow \text{wollastonite} + CO_2$$

occurs in the marble to buffer the fluid composition at $X_{CO_2} = 0.5$. We also assume that the pelite originally contained 5 wt percent H_2O (the average water content of shales) and underwent *complete* dehydration with all H_2O passing through the marble. Calculations show that in order to convert the calcite + quartz completely to wollastonite, and, hence, to lose the buffer assemblage in the marble, water from at least an equivalent volume of pelite would be required. Indeed, even larger volumes of pelite would be required than shown by these calculations, since schists retain some water in hydrous phases. Thus, even a modest amount of quartz in the marble would provide an appreciable buffer capacity. Complete buffering could occur in an interbedded sequence of marble + pelite where there is more marble than pelite.

In graphite-bearing systems, external control of fluid composition may not necessitate influx of H_2O and CO_2 from surrounding domains. For example, in the case of a thin graphite-bearing marble in a thick pelitic schist sequence the pelite could control the composition of the fluid in the marble by diffusion of hydrogen.

The importance of permeability in controlling the mineral assemblage is illustrated by Morgan (1970), where eclogite and amphibolite occur interlayered with metasedimentary rocks. Calculation of the fluid composition in the graphite-bearing metasediments shows that during metamorphism f_{H_2O} would have been sufficient to convert eclogite into amphibolite. Thus, he interprets the eclogite to represent the product of dry[17] metamorphism of basalt without influx of hydrous fluids from surrounding rocks. Local conversion of eclogite to amphibolite is believed to have occurred where hydrous fluids gained access to the basic rocks, especially along shear zones. Another example of the importance of permeability in controlling the chemistry of the pore fluid is in zeolite facies assemblages where relatively high porosity accounts for the fact that such systems are open to volatiles (A. B. Thompson, 1971, p. 153). To some extent, porosity and permeability have opposing effects on buffering. Diminishing porosity means less fluid, and, hence, less reaction necessary to control the chemistry of the pore fluid. However, lower porosity results in a decrease in permeability which may throttle the expulsion of fluids that is necessary to maintain buffering in a system with constant porosity.

No generalizations can be made from the above discussion as to open *vs* closed behavior of metamorphic systems with regard to CO_2 and H_2O. However, many recent petrologic analyses of meta-

[16] Using Hewitt's (1973a) field example as a base, Vidale and Hewitt (1973) have outlined a hypothetical example of calc-silicate zonation produced by a gradient in pore fluid composition.

[17] For kinetic reasons, some may argue against *completely* dry metamorphism of basalt to coarse-grained eclogite at moderate temperatures; however, if a fluid was present, it undoubtedly had a very low f_{H_2O} (Fry and Fyfe, 1971). The presence of a fluid phase is supported by what appear to be small fluid inclusions in a sample of California eclogite studied by Champness, Fyfe, and Lorimer (1974).

morphosed carbonate rocks suggest internal control of volatile activities through prograde reactions buffering the fluid composition. In view of the fact that at any time during metamorphism the proportion of solids far outweighs the amount of fluid, it is expected that buffering of the fluid should be rather common. A particular rock unit may experience both behaviors during its metamorphic history. Local *vs* external control of the chemical potentials of fluid components involves a complex interplay of variables that include reaction rates, permeability, amount of reactants per unit volume of rock, and the stoichiometry of the particular reaction(s) occurring (especially the number of moles of gaseous species involved in the balanced reaction). Clearly, each geologic system should be evaluated independently, with careful description of the assemblages, reaction textures, and "plumbing system," of the particular rock system. Detailed analysis of the prograde development of a rock sequence could be very instructive as to the behavior of volatiles during metamorphism.

Mixed-volatiles clearly play a very important role in metamorphism. The concept of metamorphic grade based on temperature alone is thus an oversimplification. Indeed, variations in the fluid composition may produce a "high grade" assemblage (*e.g.*, wollastonite) at lower temperatures than a "low grade" assemblage (*e.g.*, calcite + quartz). Consideration of the role of mixed volatiles may explain what might otherwise be puzzling anomalies in isograd sequences, such as, for example, Carmichael (1970) postulated for the crossing of isograds in pelitic and calcareous rocks in a Barrovian metamorphic sequence in Ontario.

Mixed Volatiles and Metasomatism

One of the most obvious environments for the occurrence of H_2O-CO_2 mixtures is in skarns formed at the contact between granitic plutons and carbonate wall rocks. Nokleberg (1973) calculated the fluid species resulting from mixing of H_2O and CO_2 in skarn environments, and he suggested several petrologic consequences of such mixing. Skarns in the Sierra Nevada contain abundant garnet that is rich in the grossularite molecule (Nokleberg, 1970; Kerrick, in progress). Assuming temperatures at the contact in the order of 700°C, and total pressure of 1–2 kbar (Kerrick, 1970), grossularite would imply relatively H_2O-rich fluids (Fig. 12). Retrograde hydrous skarn minerals, such as zoisite and prehnite, imply the persistence of H_2O-rich fluids into the waning stages of skarn formation. Knowledge of fluid composition from silicate assemblages can thus help elucidate the physicochemical conditions of skarn formation. For example, an estimate of the CO_2/H_2O ratio in the fluid aids in estimating the concentrations of some components dissolved in the fluid emanating from the adjacent intrusive (Shettel, 1973), and to explain the physicochemical controls on the deposition of some economically important minerals such as scheelite (Nokleberg, 1970).

Buffer assemblages are rare in skarns; hence, the mineralogy appears to reflect open conditions with regard to CO_2 and H_2O. The relatively H_2O-rich fluids implied by silicate assemblages suggest that influx of H_2O from the adjacent intrusive exercised a dominant control on the fluid composition. Thus, large amounts of externally derived H_2O precluded local buffering of the fluid. Burt (1971) also concluded external control of fluid components in considering redox equilibria in Fe-rich skarns. Many skarns in the Sierra Nevada show distinct mineralogical zoning parallel to the metamorphic-plutonic contact. In these skarns solid solution minerals, such as garnet and pyroxene, have the same composition within each zone, but distinctly different compositions between adjacent zones (Nokleberg, 1970; Kerrick, in progress). This is best described by Korzhinskii's (1970) model of "infiltration" metasomatism, whereby there were distinct differences in composition of the fluids between zones (*i.e.*, sharp metasomatic "fronts"). Thus, although buffering was apparently ineffective in many skarns, there may have been local variation in the fluid composition. A recent account of the theory behind infiltration *vs* diffusion metasomatism is provided by Hofmann (1972).

Rodingites form a rare but interesting calc-silicate assemblage associated with metamorphosed ultramafic rocks. In some cases, there is clear-cut evidence of metasomatic formation of rodingites at the borders of alpine ultramafic intrusions (Chidester, 1968) or near contacts between gabbro and ultramafic rocks (O'Brien and Rodgers, 1973). From the *T-X* topologies for the system CaO-Al_2O_3-SiO_2-CO_2-H_2O the presence of phases such as grossularite[18] (Olsen, 1961), prehnite (Liou, 1971b; O'Brien and

[18] Chemical analysis by E. Olsen (personal communication) shows that the grossularite from rodingites at Asbestos, Quebec, is anhydrous and very aluminous (grossularite$_{95}$–almandine$_5$).

Rodgers, 1973), wollastonite (Gresens, 1966; Olsen, 1961), and xonotolite (Smith, 1954; O'Brien and Rodgers, 1973), in some rodingites is suggestive of H_2O-rich fluids. Because of possible topologic changes with pressure, this conclusion may not hold if, as believed by some (Barnes and O'Neil, 1969), rodingites formed as a product of very low pressure (near surface) conditions that accompany serpentinization. Nevertheless, application of equilibria in the system MgO-SiO_2-CO_2-H_2O to alpine ultramafics, and of equilibria in the system CaO-Al_2O_3-SiO_2-CO_2-H_2O to assemblages in associated rodingites, could lead to a fruitful investigation of the metasomatic history of ultramafics. Some progress in using mixed-volatile equilibria in deducing the composition of metasomatic fluids permeating ultramafics has been made by Johannes (1969) and by Evans and Trommsdorff (1974).

Remaining Problems with Mixed-Volatile Equilibria

As in any field of scientific endeavor, further problems are uncovered in the light of present and past research. In this section we will outline some problems that remain with mixed-volatile equilibria.

Thermodynamic Data

Primary barriers in the accurate construction of T-X_{CO_2} diagrams from thermochemical data stem from the lack of the following data:

(a) activities of many solid solutions,
(b) high temperature heat capacities of some important rock-forming minerals (*e.g.*, zoisite, tremolite, dolomite), and
(c) activities of components in gas mixtures over a wide range of P and T.

Although vibrational entropies of phases are measured calorimetrically, considerable work remains in determining configurational entropies of some minerals. Al/Si disorder must be taken into account in computing the entropies of aluminous phases such as feldspars, amphiboles, and micas. Burnham (1973) presents an excellent general discussion of disorder in rock-forming minerals. The importance of Al/Si disorder in mixed-volatile equilibria involving aluminous phases is illustrated by the muscovite + quartz reaction shown in Figure 4b. The curve extrapolated with ordered K-feldspar (microcline) is significantly different than that with the disordered polymorph (sanidine). Furthermore, D. R. Waldbaum (personal communication) suggests that the entropy of muscovite as given by Robie and Waldbaum (1968) should be increased by about 4.5 entropy units to account for Al/Si disorder in the calorimetrically-measured samples. For exact thermodynamic extrapolation of a reaction accounting for disorder, we need to know the degree of disorder as a function of temperature (*e.g.*, Greenwood, 1972) which could then be included in Eq. (g). Useful input on this subject would come from field studies where the degree of disorder is correlated with metamorphic grade. A notorious difficulty in experimental studies is the growth of phases which do not represent the most stable state of disorder for that P-T condition. In this regard the activity data of Orville (1972) for plagioclase at 700°C and 2 kbar refers to a largely disordered albite component, and there is no guarantee that his data refers to the most stable degree of disorder under these conditions.

Hopefully, the recent book by Saxena (1973) will inspire further investigations on the thermodynamic properties of rock-forming solid solutions. In order to accurately calculate the effect of solid solution on the displacement of T-X equilibria, activity data are needed for solid solutions over a wide range of temperature. Considerable thermodynamic data for rock-forming solid solutions should arise from spectroscopic determinations of site fractionation in synthetic and natural solid solutions as a function of temperature (*e.g.*, Saxena and Ghose, 1971). Miscibility gaps of solid solutions at low to moderate metamorphic grade will further complicate the relevant T-X equilibria involving these phases. Crawford (1972) illustrates the complexities introduced by unmixing in plagioclase. Epidote and calcic-amphibole, which are involved in numerous mixed-volatile equilibria (Fig. 12, 14), are commonly unmixed in natural assemblages (*e.g.*, Hietanen, 1974). Because of the marked departure from ideal mixing, it is especially important to obtain thermodynamic data for unmixed solid solutions. Derivation of thermodynamic properties by application of solution theories to binary solvi (*e.g.*, Luth and Fenn, 1973; Warner and Luth, 1973, 1974) provides useful input in this regard. For many phases of importance in mixed-volatile equilibria, we must consider the *combined* effects of solid solution and disorder on the T-X topologies. Waldbaum (1973) presents an analysis of the combined entropy effects of solid solution and disorder of gehlenite, which is involved in some high temperature equilibria shown in Figure 12.

From current research by C. Wayne Burnham and co-workers at the Pennsylvania State University, we can expect accurate thermodynamic data for H_2O-CO_2 mixtures over a wide range of temperature and pressure. However, uncertainties will remain regarding the thermodynamic properties of gas species in fluids other than binary H_2O-CO_2 mixtures. Complex gas mixtures could be investigated with thermodynamic solution theories (King, 1969), possibly coupled with spectroscopic data (Tödheide, 1972). However, analysis of available thermodynamic data for H_2O-CO_2 mixtures using solution models (Barron, 1973) is not particularly encouraging. The thermodynamic properties of gas species in complex fluids could also be derived by careful investigations of the displacement of heterogeneous equilibria on T-X projections (*e.g.*, Fig. 8) as a function of varying activities of the gas species.

Our current model of the petrogenetic grid is based on thermodynamic calculations and experimental data involving "bulk" gases at elevated pressure and temperature. However, a major uncertainty remains in the thermodynamic properties of volatile components as thin intergranular films or as adsorbed species at grain boundaries. Little work on this subject has appeared in the geologic literature since the discussion of Fyfe, Turner, and Verhoogen (1958, p. 40–44). However, the topic of adsorbed fluids had recently been a lively source of debate amongst chemists as the controversial "polywater" concept (Lippincott *et al*, 1969; Rousseau, 1971). It would be very useful to devise high pressure, high temperature experiments measuring the properties of fluids at grain boundaries in interlocking solid aggregates. Useful information on this topic may come from experimental studies of the thermodynamic properties of thin layers of gases adsorbed on solid surfaces (*e.g.*, Day, Parfitt, and Peacock, 1974). Detailed analyses of grain boundary phenomena have recently been carried out by ceramists and metallurgists (*e.g.*, Gleiter and Chalmers, 1972). Elliott (1973) presents a recent integration of such grain-boundary phenomena in the study of rock systems.

Experimental Studies

With reliable, narrow equilibrium brackets derived from experimental work on a few key reactions, rather accurate T-X topologies can be constructed with reliable thermochemical data. Indeed, as shown in Figure 4, the largest source of error in the extrapolation of T-X equilibria usually results from the total temperature error in the experimentally determined equilibrium bracket. With cold-seal and internally heated pressure vessels, equilibrium brackets for most devolatilization reactions can be determined to an accuracy of $\pm$ 10°C. With particularly sensitive reaction monitors, such as scanning electron microscopy (Gordon, 1971; Haas, 1972), coupled with careful control and measurement of pressure and temperature during runs, it should be possible to improve the accuracy of such equilibrium brackets to $\pm$ 5°C.

In view of the interpretive problems with any one experimental technique, as outlined previously, reaction direction should be monitored by several independent techniques. Furthermore, it is important to fully characterize the optics, chemistry, and structural state of phases grown in experiments. An example of the necessity of such characterization is illustrated by the fact that synthetic pyrophyllites may differ considerably in their chemistry, which could explain some discrepancies in experimental studies on pyrophyllite stability (Rosenberg, 1974). Because the electron microprobe is capable of obtaining acceptable quantitative analyses on particles $\geq$ 1 micron in diameter, fine-grained experimental run products cannot be analyzed with this instrument. With improvements in the quantitative capabilities of non-dispersive detectors we can expect somewhat more accurate chemical analyses on fine materials using the scanning electron microscope in static mode.

In graphite-bearing experimental systems, major potential sources of error lie in the calculated gas compositions, possible kinetic problems with solid-state buffers, and slow diffusion of hydrogen through capsule walls (Huebner, 1971). Uncertainties in f_{O_2} of solid-state buffers could be eliminated with the use of a "Shaw Membrane" (Shaw, 1967). To check on the accuracy of calculated gas compositions in graphite-bearing experimental systems, it would be useful to carry out a detailed chemical analysis of the gas species over a wide range of pressure and temperature. Additional investigations of hydrogen diffusion rates as a function of thickness and composition of capsule material are clearly warranted. In order to calculate gas fugacities in natural graphite-bearing systems, it is important to obtain f_{O_2}-T information on natural assemblages. Recent experimental and thermodynamic investigations on f_{O_2} monitors of metamorphic assemblages is encouraging (*e.g.*, Rumble, 1973; Rutherford,

1969; Liou, 1973). Solid electrolyte fugacity sensors offer an intriguing possibility of determining the f_{O_2} and T of crystallization of a mineral assemblage (Sato, 1971).

Aside from Fe-bearing phases, there are other minerals whose compositions are sensitive to variations in the activities of gas components. Potential monitors of fugacities of halogen species include apatite and phlogopite (Stormer and Carmichael, 1971; Munoz and Eugster, 1969; Munoz and Ludington, 1974). Scapolite composition may prove useful to monitor CO_2 fugacity (Marakushev, 1964). Accurate determination of the H_2O content of some hydrous phases may yield estimates of f_{H_2O} in metamorphic systems (Weisbrod, 1973). Wilkins and Sabine (1973) describe an accurate analytical technique for determining the H_2O content of silicates.

Studies of *primary* fluid inclusions in metamorphic rocks will undoubtedly offer considerable insight into mixed-volatile equilibria (*e.g.*, Roedder, 1972). The next few years will see a marked increase in the number of papers on fluid inclusion studies in metamorphic rocks.

Isotopic investigations of minerals offers a promising approach to deducing fluid composition during metamorphism. Since there are significant differences in the isotopic fractionation factors between various gas species in the system C–O–H (Bottinga, 1969), the isotopic composition of solids in equilibrium with these fluids should reflect changes in fluid composition. Experimental measurements related to this are in progress by H. Ohmoto at the Pennsylvania State University. Experimental data related to fractionation factors as a function of fluid composition could then be tested on field examples with independent evidence of fluid composition obtained by the application of T-X equilibria or by fluid inclusion studies.

Kinetic studies of devolatilization reactions (Kridelbaugh, 1973) will be very important in evaluating the effectiveness of buffering in metamorphic systems. In view of the fact that true buffering at constant porosity requires adequate migration of volatiles, research on fluid diffusion rates along intergranular boundaries (Greenwood, 1960) will also be of importance in kinetic arguments.

Field Investigations

In order to improve our understanding of mixed-volatile equilibria in metamorphic systems, one should integrate independent monitors of temperature, pressure, and fluid composition. Geothermometry obtained by application of the dolomite-calcite solvus to metacarbonate assemblages (Hutcheon and Moore, 1973; Sobol and Essene, 1973) is very useful to integrate with the application of T-X diagrams. Indeed, such independent geothermometry has considerable potential in sorting out controversy regarding T-X topologies (Slaughter, Kerrick, and Wall, 1974). Independent evidence of fluid composition could be gained by fluid inclusion analysis and by isotopic fractionation between coexisting phases, as previously outlined.

There is considerable uncertainty with regard to pressure estimates in metamorphic systems. Combined experimental and thermodynamic investigations of the pressure effect on T-X topologies (*e.g.*, Fig. 13) offers considerable potential for geobarometry. Because of uncertainty in pressure estimates, there is a need to integrate other independent sources of geobarometry in natural systems, such as depth of burial estimates, and pressure estimates based on solid-solid reactions (*e.g.*, Al_2SiO_5 polymorphs, Holdaway, 1971; sulfide equilibria, Scott and Barnes, 1971).

The role of solid solution must be carefully evaluated in field investigations of mixed-volatile equilibria. It will be instructive to follow compositional changes of solid solutions as a function of gradients in activities of gas species (*e.g.*, Hewitt, 1973b, p. 453–454), and in prograde metamorphism (*e.g.*, Kerrick, Crawford, and Randazzo, 1973, p. 309; Hewitt, 1973a, p. 465; Frey and Orville, 1974). Such studies will provide improved knowledge of the model of buffered equilibria, as well as better understanding of the role of solid solution in mixed-volatile equilibria.

The controls of fluid composition must be determined on all scales. Careful sampling across interbedded lithologies and across veins will aid in determining volatile activity gradients in rock systems. Analysis of the prograde metamorphism of interbedded lithologies with regard to fluid mixing would be particularly helpful. With careful petrologic descriptions leading to calculation of the amount of volatiles given off by a particular lithologic unit (*e.g.*, Carmichael, 1970, p. 173–177) coupled with isotopic investigations (*e.g.*, Shieh and Taylor, 1969), accurate mass-balance calculations of fluid mixing will be possible for rock systems. Sophisticated metasomatic theory with regard to volatile species (*e.g.*, Mueller, 1967) will be necessary to integrate

with such an analysis. More work needs to be carried out on mixed-volatile equilibria on the megascopic scale. Detailed mapping of isograds with regard to interbedded lithologies will clarify gradients in the volatile activities (*e.g.*, Carmichael, 1970; P. H. Thompson, 1973).

The role of non-binary C–O–H fluids in metamorphism could be profitably approached by field investigations of graphite-bearing rocks. Petrologic analysis of interbedded graphite-bearing and graphite-free lithologies would be instructive in this regard.

Finally, it would be fruitful to carry out field investigations to test for "vapor-absence" in metamorphic systems. Watts (1973) presents a field-oriented analysis of the relationship between vapor-present and vapor-absent equilibria in the system $CaO–MgO–Al_2O_3–SiO_2–CO_2–H_2O$. In this regard, it would be profitable to analyze rock systems with $\mu_{H_2O} - \mu_{CO_2}$ diagrams rather than *T-X* plots, since the latter (as conventionally used) are applicable only to vapor-saturated systems.

Acknowledgments

I am very grateful to F. D. Bloss, A. L. Boettcher, D. M. Carmichael, E. J. Essene, J. R. Holloway, and particularly David R. Waldbaum for critically reviewing an early draft of this paper. I also thank my graduate students J. A. Hunt, J. N. Moore, and J. Slaughter, for their helpful comments. This work was supported by N. S. F. Grant GA25685.

References

ALBEE, A. L., AND E-AN ZEN (1969) Dependence of the zeolitic facies on the chemical potentials of CO_2 and H_2O. In *Physico-Chemical Petrology*, V.I.V.A. Zharikov, Ed., Akademi Nauk U.S.S.R., p. 249–260.

ALTHAUS, E. (1968) Der einfluss des wassers auf metamorphe mineral reaktionen. *Neues Jahrb. Mineral. Monatsh.* **9,** 289–306.

———, E. KAROTKE, K. H. NITSCH, AND H. G. F. WINKLER (1970) An experimental re-examination of the upper stability limit of muscovite plus quartz. *Neues Jahrb. Mineral. Monatsh.* **7,** 325–336.

ANDERSON, G. M., AND C. WAYNE BURNHAM (1965) The solubility of quartz in super-critical water. *Am. J. Sci.* **263,** 494–511.

BARNES, I., AND J. R. O'NEIL (1969) The relationship between fluids in some fresh alpine-type ultramafics and possible modern serpentinization, Western United States. *Bull. Geol. Soc. Am.* **80,** 1947–1960.

BARRON, L. M. (1973) Nonideal thermodynamic properties of H_2O-CO_2 mixtures for 0.4–2 kb, and 400–700°C. *Contrib. Mineral. Petrol.* **39,** 184.

——— (1974) Template plotting of reactions involving water-carbon dioxide minerals. *Contrib. Mineral. Petrol.* **44,** 81–83.

BECKER, P., AND G. HOSCHEK (1973) Experimentelle bildung von klinohumit. *Neues Jahrb. Mineral. Monatsh.* **6,** 281–287.

BOETTCHER, A. L. (1970) The system CaO-Al_2O_3-SiO_2-H_2O at high pressures and temperatures. *J. Petrol.* **11,** 337–379.

———, AND D. M. KERRICK (1971) Temperature calibration in cold-seal vessels. In, G. C. Ulmer, Ed., *Research Techniques for High Pressure and High Temperature,* Springer Verlag, New York, p. 179–193.

BOTTINGA, Y. (1969) Calculated fractionation factors for carbon and hydrogen isotope exchange in the system calcite-carbon dioxide-graphite-methane-hydrogen-water vapor. *Geochim. Cosmochim. Acta,* **33,** 49–64.

BUCKNER, D. A., D. M. ROY, AND R. ROY (1960) Studies in the system CaO-Al_2O_3-SiO_2-H_2O. II. The system $CaSiO_3$-H_2O. *Am. J. Sci.* **258,** 132–147.

BUDDINGTON, A. F., AND D. H. LINDSLEY (1964) Iron-titanium oxide minerals and synthetic equivalents. *J. Petrol.* **5,** 310–357.

BURNHAM, C. WAYNE, J. R. HOLLOWAY, AND N. F. DAVIS (1969) Thermodynamic properties of water to 1000°C and 10,000 bars. *Geol. Soc. Am. Spec. Pap.* **132,** 96 pp.

BURNHAM, CHARLES W. (1973) Order-disorder relationships in some rock-forming silicate minerals. *Annu. Rev. Earth Planet. Sci.* **1,** 313–338.

BURT, D. M. (1971) Some phase equilibria in the system Ca-Fe-Si-C-O. *Carnegie Inst. Wash. Year Book,* **70,** 178–184.

——— (1972a) Decarbonation sequence in the system $CaO–MnO–SiO_2–CO_2$. *Carnegie Inst. Wash. Year Book,* **71,** 427–435.

——— (1972b) The system Fe–Si–C–O–H: a model for metamorphosed iron formations. *Carnegie Inst. Wash. Year Book,* **71,** 435–443.

——— (1972c) The influence of fluorine on the facies of Ca–Fe–Si skarns. *Carnegie Inst. Wash. Year Book,* **71,** 443–450.

——— (1972d) Silicate–sulfide equilibria in Ca-Fe-Si skarn deposits. *Carnegie Inst. Wash. Year Book,* **71,** 450–457.

CARMICHAEL, D. M. (1970) Intersecting isograds in the Whetstone Lake area, Ontario. *J. Petrol.* **11,** 147–181.

CERMIGNANI, C., AND G. M. ANDERSON (1973) Origin of a diopside–tremolite assemblage near Tweed, Ontario. *Can. J. Earth Sci.* **10,** 84–90.

CHAMPNESS, P. E., W. S. FYFE, AND G. W. LORIMER (1974) Dislocations and voids in pyroxene from a low-temperature eclogite: mechanism of eclogite formation. *Contrib. Mineral. Petrol.* **43,** 91–98.

CHATTERJEE, N. D. (1971) Phase equilibria in the alpine metamorphic rocks of the environs of the Dora-Maira-Massif, Western Italian Alps. *Neues Jahrb. Mineral. Abh.,* **114,** 181–245.

CHIDESTER, A. H. (1968) Evolution of the ultramafic complexes of northwestern New England. In, E-An Zen, W. S. White, and J. B. Hadley, Eds., *Studies of Appalachian Geology: Northern and Maritime.* Interscience, New York, pp. 343–354.

COOMBS, D. S., A. J. ELLIS, W. S. FYFE, AND A. M. TAYLOR (1959) The zeolite facies, with comments on the inter-

pretation of hydrothermal synthesis. *Geochim. Cosmochim. Acta,* **17,** 53–107.

———, R. J. NORODYSKI, AND R. S. NAYLOR (1970) Occurrence of prehnite-pumpelleyite facies metamorphism in northern Maine. *Am. J. Sci.* **268,** 142–156.

CRAWFORD, M. L. (1972) Plagioclase and other mineral equilibria in a contact metamorphic aureole. *Contrib. Mineral. Petrol.* **36,** 293–314.

DAY, R. E., G. D. PARFITT, AND J. PEACOCK (1974) The differential enthalpies and entropies of adsorption of water vapor on rutile at 25°C in the region of monolayer coverage. *J. Colloid Interface Sci.* **46,** 17–21.

ELLIOTT, D. (1973) Diffusion flow laws in metamorphic rocks. *Geol. Soc. Am. Bull.* **84,** 2645–2664.

ERNST, W. G. (1972) CO_2-poor composition of the fluid attending Franciscan and Sanbagawa low-grade metamorphism. *Geochim. Cosmochim. Acta,* **36,** 497–504.

ESSENE, E. J., AND W. S. FYFE (1967) Omphacite in Californian rocks. *Contrib. Mineral. Petrol.* **15,** 1–23.

EUGSTER, H. P., AND G. B. SKIPPEN (1967) Igneous and metamorphic reactions involving gas equilibria. In, P. H. Abelson, Ed., *Researches in Geochemistry,* II, John Wiley and Sons, New York, p. 492–520.

EVANS, B. W. (1965) Application of a reaction-rate method to the breakdown equilibria of muscovite and muscovite plus quartz. *Am. J. Sci.* **263,** 647–667.

———, AND V. TROMMSDORFF (1974) Stability of enstatite + talc, and CO_2-metasomatism of metaperidotite, Val d'Efra, Lepontine Alps, *Am. J. Sci.* **274,** 274–296.

FINGER, L. W., AND D. M. BURT (1972) REACTION, a Fortran IV computer program to balance chemical reactions. *Carnegie Inst. Wash. Year Book,* **71,** 616–620.

FRENCH, B. M. (1966) Some geological implications of equilibrium between graphite and a C–H–O gas phase at high temperatures and pressures. *Rev. Geophys.* **4,** 223–253.

FREY, M., AND P. M. ORVILLE (1974) Plagioclase in margarite-bearing rocks. *Am. J. Sci.* **274,** 31–47.

FRY, N., AND W. S. FYFE (1971) On the significance of the eclogite facies in Alpine metamorphism. *Verh. Geol.* **B.-A.,** 257–265.

FYFE, W. S., F. J. TURNER, AND J. VERHOOGEN (1958) Metamorphic reactions and metamorphic facies. *Geol. Soc. Am. Mem.* **73,** 259 pp.

GARRELS, R. M., AND C. L. CHRIST (1965) *Solutions, Minerals, and Equilibra.* Harper and Row, New York. 450 p.

GHENT, E. D., J. W. JONES, AND J. NICHOLLS (1970) A note on the significance of the assemblage calcite–quartz–plagioclase–paragonite–graphite. *Contrib. Mineral. Petrol.* **28,** 112–116.

———, AND C. D. S. DEVRIES (1972) Plagioclase–garnet–epidote equilibria in hornblende–plagioclase bearing rocks from the Esplanade Range, British Columbia. *Can. J. Earth Sci.* **9,** 618–635.

GLASSLEY, W. (1974) A model for phase equilibria in the prehnite–pumpelleyite facies. *Contrib. Mineral. Petrol.* **43,** 317–332.

GLEITER, H., AND B. CHALMERS (1972) High angle grain boundaries. In, B. Chalmers, J. W. Christian, and T. B. Massalski, Eds., *Progress in Materials Science,* **16,** 274 p.

GORDON, T. M. (1971) Some observations on the formation of wollastonite from calcite and quartz. *Can. J. Earth Sci.* **8,** 844–851.

——— (1973) Determination of internally consistent thermodynamic data from phase equilibrium experiments. *J. Geol.* **81,** 199–208.

———, AND H. J. GREENWOOD (1970) The reaction: dolomite + quartz + water = talc + calcite +carbon dioxide. *Am. J. Sci.* **268,** 225–242.

———, AND ——— (1971) Stability of grossularite in H_2O–CO_2 mixtures. *Am. Mineral.* **56,** 1674–1688.

GREENWOOD, H. J. (1960) Water pressure and total pressure in metamorphic rocks. *Carnegie Inst. Wash. Year Book,* **59,** 58–63.

——— (1961) The system $NaAlSi_2O_6$-H_2O-Argon: total pressure and water pressure in metamorphism. *J. Geophys. Res.* **66,** 3923–3946.

——— (1962) Metamorphic reactions involving two volatile components. *Carnegie Inst. Wash. Year Book,* **61,** 82–85.

——— (1967a) Mineral equilibria in the system MgO–SiO_2–H_2O–CO_2. In, P. H. Abelson, Ed., *Researches in Geochemistry,* II. John Wiley and Sons, New York, p. 542–547.

——— (1967b) Wollastonite: stability in H_2O–CO_2 mixtures and occurrence in a contact–metamorphic aureole near Salmo, British Columbia, Canada. *Am. Mineral.* **52,** 1669–1680.

——— (1972) Al^{IV}–Si^{IV} disorder in sillimanite and its effect on phase relations of the aluminum silicate minerals. *Geol. Soc. Am. Mem.* **132,** p. 533–571.

——— (1973) Thermodynamic properties of gaseous mixtures of H_2O and CO_2 between 450°C and 800°C and 0–500 bars. *Am. J. Sci.* **273,** 561–571.

GRESENS, R. L. (1966) Wollastonite in rodingites from Cape San Martin. *Geol. Soc. Am. Spec. Pap.* **87,** 66.

GUIDOTTI, C. V. (1970) The mineralogy and petrology of the transition from the lower to upper sillimanite zone in the Oquossoc Area, Maine. *J. Petrol.* **11,** 277–336.

HAAS, H. (1972) Diaspore–corundum equilibrium determined by epitaxis of diaspore on corundum. *Am. Mineral.* **57,** 1375–1385.

HARKER, R. I., AND O. F. TUTTLE (1956) Experimental data on the P_{CO_2}–T curve for the reaction: calcite + quartz = wollastonite + CO_2. *Am. J. Sci.* **254,** 239–256.

HEARD, H. C. (1963) Effect of large changes in strain rate in the experimental deformation of Yule Marble. *J. Geol.* **71,** 162–195.

HEWITT, D. A. (1973a) Stability of the assemblage muscovite — calcite — quartz. *Am. Mineral.* **58,** 785–791.

——— (1973b) The metamorphism of micaceous limestones from south-central Connecticut. *Am. J. Sci.* **273A,** 444–469.

HIETANEN, A. (1974) Amphibole pairs, epidote minerals, chlorite, and plagioclase in metamorphic rocks, Northern Sierra Nevada, California. *Am. Mineral.* **59,** 22–40.

HOBBS, B. E. (1968) Recrystallization of single crystals of quartz. *Tectonophysics,* **6,** 353–401.

HOFMANN, A. (1972) Chromatographic theory of infiltration metasomatism and its application to feldspars. *Am. J. Sci.* **272,** 69–90.

HOLDAWAY, M. J. (1966) Hydrothermal stability of clinozoisite plus quartz. *Am. J. Sci.* **264,** 643–667.

——— (1971) Stability of andalusite and the aluminum silicate phase diagram. *Am. J. Sci.* **271,** 97–131.

——— (1972) Thermal stability of Al–Fe epidote as a function of f_{O_2} and Fe content. *Contrib. Mineral. Petrol.* **37,** 307–340.

HOLLOWAY, J. R., C. W. BURNHAM, AND G. L. MILLHOLLEN (1968) Generation of H_2O-CO_2 mixtures for use in hydrothermal experimentation. *J. Geophys. Res.* **73,** 6958–6600.

———, AND R. L. REESE (1974) The generation of N_2-CO_2-H_2O fluids for use in hydrothermal experimentation. I. Experimental method and equilibrium calculations in the C–O–H–N system. *Am. Mineral.* **59,** 587–597.

HOSCHEK, G. (1973) Die reaktion Phlogopit + Calcit + Quarz = Tremolit + Kalifeldspar + H_2O + CO_2. *Contrib. Mineral. Petrol.* **39,** 231–237.

HUEBNER, J. S. (1971) Buffering techniques for hydrostatic systems at elevated pressures. In, G. C. Ulmer, Ed., *Research Techniques for High Pressure and High Temperature,* Springer Verlag, New York, p. 123–177.

HUTCHEON, I., AND J. M. MOORE (1973) The tremolite isograd near Marble Lake, Ontario. *Can. J. Earth Sci.* **10,** 936–947.

JOHANNES, W. (1969) An experimental investigation of the system MgO-SiO_2-H_2O-CO_2. *Am. J. Sci.* **267,** 1083–1104.

———, AND P. M. ORVILLE (1972) Zur stabilitat der mineral paragenesen muskovit + calcit + quarz, zoisit + muskovit + quarz, anorthit + K-feldspar und anorthit + calcit. *Fortschr. Mineral.* **50,** 47.

JONES, J. W. (1972) An almandine garnet isograd in the Rogers Pass Area, British Columbia: the nature of the reaction and an estimation of the physical conditions during its formation. *Contrib. Mineral. Petrol.* **37,** 291–306.

KENNEDY, G. C. (1954) Pressure-volume-temperature relations in CO_2 at elevated temperatures and pressures. *Am. J. Sci.* **252,** 225–241.

KERRICK, D. M. (1968) Experiments on the upper stability limit of pyrophyllite at 1.8 kilobars and 3.9 kilobars water pressure. *Am. J. Sci.* **266,** 204–214.

——— (1970) Contact metamorphism in some areas of the Sierra Nevada, California. *Geol. Soc. Am. Bull.* **81,** 2913–2938.

——— (1972) Experimental determination of muscovite + quartz stability with $P_{H_2O} < P_{total}$. *Am. J. Sci.* **272,** 946–958.

———, AND W. R. COTTON (1971) Stability relations of jadeite pyroxene in Franciscan metagraywackes near San Jose, California. *Am. J. Sci.* **271,** 350–369.

———, K. E. CRAWFORD, AND A. F. RANDAZZO (1973) Metamorphism of calcareous rocks in three roof pendants in the Sierra Nevada, California. *J. Petrol.* **14,** 303–325.

———, J. A. HUNT, AND V. J. WALL (1973) Experiments on some equilibria involving calc-silicate phases (abstr.). *Geol. Soc. Am. Abstr. Program,* **5,** 693.

KING, M. B. (1969) *Phase Equilibrium in Mixtures.* Pergamon Press, 584 p.

KORZHINSKII, D. S. (1959) *Physicochemical Basis of the Analysis of the Paragenesis of Minerals.* Consultants Bureau, New York.

——— (1967) On thermodynamics of open systems and the phase rule (A reply to the second critical paper of D. F. Weill and W. S. Fyfe). *Geochim. Cosmochim. Acta,* **30,** 829–835.

——— (1970) *Theory of Metasomatic Zoning.* Oxford, Clarendon Press, 162 p.

KRIDELBAUGH, S. J. (1973) The kinetics of the reaction: calcite + quartz = wollastonite + carbon dioxide at elevated temperatures and pressures. *Am. J. Sci.* **273,** 757–777.

LIOU, J. G. (1970) Synthesis and stability relations of of wairakite, $CaAl_2Si_4O_{12}\cdot 2H_2O$. *Contrib. Mineral. Petrol.* **27,** 259–282.

LIOU, J. G. (1971a) *P-T* stabilities of laumontite, wairakite, lawsonite, and related minerals in the system: $CaAl_2Si_2O_8$-SiO_2-H_2O. *J. Petrol.* **12,** 379–411.

——— (1971b) Synthesis and stability relations of prehnite $Ca_2Al_2Si_3O_{10}(OH)_2$. *Am. Mineral.* **56,** 507–531.

——— (1973) Synthesis and stability relations of epidote, $Ca_2Al_2FeSi_3O_{12}$. *J. Petrol.* **14,** 381–413.

LIPPINCOTT, E. R., R. S. STROMBERG, W. H. GRANT, AND G. L. CESSAC (1969) Polywater. *Science,* **164,** 1482–1487.

LUTH, W. C., AND P. M. FENN (1973) Calculation of binary solvi with special reference to the sanidine-high albite solvus. *Am. Mineral.* **58,** 1009–1015.

MARAKUSHEV, A. A. (1964) Analysis of scapolite paragenesis. *Geochem. Int.* **1,** 114–126.

MELSON, W. G. (1966) Phase equilibria in calc-silicate hornfels, Lewis and Clark County, Montana. *Am. Mineral.* **51,** 402–421.

METZ, P. (1970) Experimentelle untersuchung der metamorphose von kieselig dolomitischen sedimenten. *Contrib. Mineral. Petrol.* **28,** 221–250.

MIYASHIRO, A. (1964) Oxidation and reduction in the earth's crust with special reference to the role of graphite. *Geochim. Cosmochim. Acta,* **28,** 717–729.

MORGAN, B. A. (1970) Petrology and mineralogy of eclogite and garnet amphibolite from Puerto Cabello, Venezula. *J. Petrol.* **11,** 101–145.

MUELLER, R. F. (1967) Mobility of the elements in metamorphism. *J. Geol.* **75,** 565–582.

MUFFLER, L. J. P., AND D. E. WHITE (1969) Active metamorphism of Upper Cenozoic sediments in the Salton Sea geothermal field and the Salton Trough, Southeastern California. *Bull. Geol. Soc. Am.* **80,** 157–182.

MUNOZ, J. L., AND H. P. EUGSTER (1969) Experimental control of fluorine reactions in hydrothermal systems. *Am. Mineral.* **54,** 943–959.

———, AND S. D. LUDINGTON (1974) Fluoride-hydroxyl exchange in biotite. *Am. J. Sci.* **274,** 396–413.

NAKAJIMA, W., AND K. TANAKA (1967) Zeolite-bearing tuffs from the Izumi Group in the central part of the Izumi mountain range, Southwest Japan, with reference to mordenite tuffs and laumontite tuffs. *J. Geol. Soc. Japan,* **73,** 273–345.

NAVROTSKY, A. (1971) The intracrystalline cation distribution and the thermodynamics of solid solution formation in the system $FeSiO_3$-$MgSiO_3$. *Am. Mineral.* **56,** 201–211.

NEWTON, R. C. (1966) Some calc-silicate equilibrium relations. *Am. J. Sci.* **264,** 204–222.

NITSCH, K.-H. (1972) Das P-T-X_{CO_2}-Stabilitatsfeld von lawsonit. *Contrib. Mineral. Petrol.* **34,** 116–134.

———, AND B. STORRE (1972) Zur stabilitat von margarit in H_2O-CO_2-gasgemischen. *Fortschr. Mineral.* **50,** 71–73.

NOKLEBERG, W. J. (1970) *Geology of the Strawberry Mine Roof Pendant, Central Sierra Nevada, California.* Ph.D. Thesis, University of California, Santa Barbara, 157 pp.

——— (1973) CO_2 as a source of oxygen in the metasomatism of carbonates. *Am. J. Sci.* **273,** 498–514.

O'BRIEN, J. P., AND K. A. RODGERS (1973) Xonotolite and rodingites from Wairere, New Zealand. *Mineral. Mag.* **39,** 233–240.

OLSEN, E. J. (1961) High temperature acid rocks associated with serpentinite in eastern Quebec. *Am. J. Sci.* **259,** 329–347.

ORVILLE, P. M. (1972) Plagioclase cation exchange equilibria with aqueous chloride solution: Results at 700°C and 2000 bars in the presence of quartz. *Am. J. Sci.* **272,** 234–272.

PETERS, TJ., H. SCHWANDER, AND V. TROMMSDORFF (1973) Assemblages among tephroite, pyroxmangite, rhodochrosite, quartz: experimental data and occurrences in the Rhetic Alps. *Contrib. Mineral. Petrol.* **42,** 325–332.

PRICE, D. (1955) Thermodynamic functions of carbon dioxide. *Ind. Eng. Chem.* **47,** 1649–1652.

PUHAN, D., AND E. HOFFER (1973) Phase relations of talc and tremolite in metamorphic calcite-dolomite sediments in the southern portion of the Damara Belt (South West Africa). *Contrib. Mineral. Petrol.* **40,** 207–214.

ROBIE, R. A., AND D. R. WALDBAUM (1968) Thermodynamic properties of minerals and related substances at 298.15 K (25°C) and one atmosphere (1.013 bars) pressure and at higher temperatures. *U.S. Geol. Surv. Bull.* **1259,** 256 pp.

ROEDDER, E. (1972) Composition of fluid inclusions. In M. Fleischer, Ed., *Data of Geochemistry,* Chap. JJ, *U.S. Geol. Surv. Prof. Pap.* **440-JJ,** 164 pp.

ROSENBERG, P. E. (1974) Pyrophyllite solid solutions in the system Al_2O_3-SiO_2-H_2O. *Am. Mineral.* **59,** 254–260.

ROUSSEAU, D. L. (1971) "Polywater" and sweat: similarities between infrared spectra. *Science,* **171,** 170–172.

RUMBLE, D. (1973) Fe-Ti oxide minerals from regionally metamorphosed quartzites of western New Hampshire. *Contrib. Mineral. Petrol.* **42,** 181–195.

RUTHERFORD, M. J. (1969) An experimental determination of iron biotite-alkali feldspar equilibria. *J. Petrol.* **10,** 381–408.

RYZHENKO, B. N., AND S. D. MALININ (1971) The fugacity rule for the systems CO_2-H_2O-CO_2-CH_4, CO_2-N_2, and CO_2-H_2. *Geochem. Int.* p. 562–574.

———, AND V. P. VOLKOV (1971) Fugacity coefficients of some gases in a broad range of temperatures and pressures. *Geochem. Int.* p. 468–481.

SATO, M. (1971) Electrochemical measurements and control of oxygen fugacity and other gaseous fugacities with solid electrolyte systems. In G. C. Ulmer, Ed., *Research Techniques for High Pressure and High Temperature,* Springer Verlag, New York, p. 43–99.

SAXENA, S. K. (1972) Retrieval of thermodynamic data from a study of inter-crystalline and intra-crystalline ion exchange equilibrium. *Am. Mineral.* **57,** 1782–1800.

——— (1973) *Thermodynamics of Rock-Forming Crystalline Solutions.* Springer Verlag, New York, 188 p.

———, AND S. GHOSE (1970) Order-disorder and the activity-composition relation in a binary crystalline solution. I. Metamorphic orthopyroxene. *Am. Mineral.,* **55,** 1219–1225.

SCOTT, S. D., AND H. L. BARNES (1971) Sphalerite geothermometry and geobarometry. *Econ. Geol.* **66,** 653–669.

SHARP, W. E. (1962) The thermodynamic functions for carbon dioxide in the range 40–1000°C and 1 to 1400 bars. University of California, Lawrence Radiation Lab. Livermore, California, UCRL-**7168,** 52 p.

SHAW, H. R. (1967) Hydrogen osmosis in hydrothermal experiments. In, P. H. Abelson, Ed., *Researches in Geochemistry,* II, John Wiley and Sons, New York, p. 542–547.

SHETTEL, D. L., JR. (1973) Solubility of quartz in H_2O-CO_2 fluids at 5kb and 500°-900°C. *Am. Geophys. Union Trans. Abstr.* **54,** 480.

SHIEH, Y. N., AND H. P. TAYLOR, JR. (1969) Oxygen and carbon isotope studies of contact metamorphism of carbonate rocks. *J. Petrol.* **10,** 307–331.

SKIPPEN, G. B. (1970) A FORTRAN IV program for the calculation of equilibrium curves on X_{CO_2}-T diagrams. *Geol. Pap.* **70-3,** Carleton University, Ottawa, Canada.

——— (1971) Experimental data for reactions in siliceous marbles. *J. Geol.* **79,** 457–481.

——— (1974) An experimental model for low pressure metamorphism of siliceous dolomitic marble. *Am. J. Sci.* **274,** 487–509.

SLAUGHTER, J., D. M. KERRICK, AND V. J. WALL (1974) Experimental and thermodynamic study of equilibria in the system CaO-MgO-SiO_2-H_2O-CO_2. *Am. J. Sci.* **274,** (in press).

SMITH, C. H. (1954) On the occurrence and origin of xonotolite. *Am. Mineral.* **39,** 531–532.

SOBOL, J. W., AND E. J. ESSENE (1973) Petrology of Grenville marbles from southern Ontario (abstr.). *Geol. Soc. Am. Abstr. Program,* **5,** 815.

STORMER, J. C., AND I. S. E. CARMICHAEL (1971) Fluorine-hydroxyl exchange in apatite and biotite: a potential igneous geothermometer. *Contrib. Mineral. Petrol.* **31,** 121–131.

STORRE, B. (1970) Stabilitatsbedingungen grossular-führenden paragenesen in system CaO-Al_2O_3-SiO_2-CO_2-H_2O. *Contrib. Mineral. Petrol.* **29,** 145–162.

———, AND K.-H. NITSCH (1972) Die reaktion 2 Zoisite + 1 CO_2 = 3 Anorthite + 1 Calcite + 1 CO_2. *Contrib. Mineral. Petrol.* **35,** 1–10.

TELL, I. (1974) Hydrothermal studies on fluorine metamorphic reactions in siliceous dolomite. *Contrib. Mineral. Petrol.* **43,** 99–110.

THOMPSON, A. B. (1970) A note on the kaolinite-pyrophyllite equilibrium. *Am. J. Sci.* **268,** 267–275.

——— (1971) P_{CO_2} in low-grade metamorphism; zeolite, carbonate, clay mineral, prehnite relations in the system CaO-Al_2O_3-SiO_2-CO_2-H_2O. *Contrib. Mineral. Petrol.* **33,** 145–161.

THOMPSON, J. B., JR. (1955) The thermodynamic basis for the mineral facies concept. *Am. J. Sci.* **253,** 65–103.

——— (1970) Geochemical reaction and open systems. *Geochim. Cosmochim. Acta,* **34,** 529–551.

THOMPSON, P. H. (1973) Mineral zones and isograds in "impure" calcareous rocks, an alternative means of evaluating metamorphic grade. *Contrib. Mineral. Petrol.* **42,** 63–80.

TÖDHEIDE, K. (1972) Water at high temperatures and pressures. In, F. Franks, Ed., *Water, a Comprehensive Treatise,* Vol. 1, p. 463–514.

———, AND E. U. FRANCK (1963) Das zweiphasengebiet und die kritische kurve im system kohlendioxid-wasser bis zu drucken von 3500 bar. *Z. Phys. Chem.* **37,** 387–401.

TROMMSDORFF, V. (1972) Change in *T-X* during metamorphism of siliceous dolomitic rocks of the Central Alps. *Schweiz. Mineral. Petrogr. Mitt.* **52,** 567–571.

———, AND V. W. EVANS (1972) Progressive metamorphism of antigorite schist in the Bergell Tonalite aureole (Italy). *Am. J. Sci.* **272,** 423–437.

VELDE, B. (1971) The stability and natural occurrence of margarite. *Mineral. Mag.* **38,** 317–323.

VIDALE, R. J., AND D. A. HEWITT (1973) "Mobile" components in the formation of calc-silicate bands. *Am. Mineral.* **58,** 991–997.

WALDBAUM, D. R. (1973) The configurational entropies of $Ca_2Mg_2Si_2O_7$-$Ca_2SiAl_2O_7$ melilites and related minerals. *Contrib. Mineral. Petrol.* **39,** 33–54.

WALL, V. J., AND E. J. ESSENE (1972) Subsolidus equilibria in CaO-Al_2O_3-SiO_2-H_2O (abstr.). *Geol. Soc. Am. Abstr. Program,* **4,** 700.

WARNER, R. D., AND W. C. LUTH (1973) Two-phase data for the join monticellite ($CaMgSiO_4$)-forsterite (Mg_2SiO_4): Experimental results and numerical analysis. *Am. Mineral.* **58,** 998–1008.

———, AND ——— (1974) The diopside-orthoenstatite two-phase regions in the system $CaMgSi_2O_6$-$Mg_2Si_2O_6$. *Am. Mineral.* **59,** 98–109.

WATTS, B. J. (1973) Relationships between fluid-bearing and fluid-absent invariant points and a petrogenetic grid for a greenschist facies assemblage in the system CaO-MgO-Al_2O_3-SiO_2-CO_2-H_2O. *Contrib. Mineral. Petrol.* **40,** 225–238.

WEILL, D. F., AND W. S. FYFE (1967) On equilibrium thermodynamics of open systems and the phase rule (A reply to D. S. Korzhinskii). *Geochim. Cosmochim. Acta,* **31,** 1167–1176.

WEISBROD, A. (1973) The problem of water in cordierite. *Carnegie Inst. Wash. Year Book,* **72,** 521–523.

WILKINS, R. W. T., AND W. SABINE (1973) Water content of some nominally anhydrous silicates. *Am. Mineral.* **58,** 508–516.

WINKLER, H. G. F. (1967) *Petrogenesis of Metamorphic* Rocks. Springer Verlag, New York, 237 pp.

WONES, D. R., AND H. P. EUGSTER (1965) Stability of biotite: experiment, theory, and application. *Am. Mineral.* **50,** 1228–1272.

WYLLIE, P. J. (1962) The effect of 'impure' pore fluids on metamorphic dissociation reactions. *Mineral. Mag.* **33,** 9–25.

ZEN, E-AN (1961) The zeolite facies: an interpretation. *Am. J. Sci.* **259,** 201–409.

——— (1963) Components, phases, and criteria of chemical equilibrium in rocks. *Am. J. Sci.* **261,** 929–942.

——— (1966) Construction of pressure-temperature diagrams for multicomponent system after the method of Schreinemakers—a geometric approach. *U.S. Geol. Surv. Bull.* **1225.**

——— (1972) Gibbs free-energy, enthalpy, and entropy of ten rock-forming minerals: calculations, discrepancies, implications. *Am. Mineral.* **57,** 524–553.

Manuscript received, November 7, 1973; accepted for publication, February 12, 1974.